THE UNIVERSITY OF SHEFFIELD

# NOD SCID MICE AS A MODEL OF PROSTATE CANCER METASTASIS TO BONE

GURUBALAN JAYADEVAN

**AUGUST 2008**

**SUPERVISOR: PROF. PETER CROUCHER**

A project dissertation in partial fulfilment of the requirements for the Master of Science degree in Molecular and Genetic Medicine of the University of Sheffield.

# ACKNOWLEDGEMENT

"It is well to give when asked, but it is better to give unasked, through understanding."
-Khalil Gibran

I would like to thank Prof. Peter Croucher for the opportunity, guidance, supervision and support offered to me throughout this project and for the successful accomplishment for the same. I would like to thank Dr. Michelle Anne Lawson for her continuous support throughout this project. I would also like to thank her for all the multiphoton work and reading multiple drafts of my thesis document. I would like to thank Anne Fowles for all the animal works and the constant source of encouragement. I would like to extend my special thanks to Dr. Les Coulton for the μCT, histomorphometry and statistical work. I would also like to thank him for all the time he spent for the discussion of my results. I would like to thank Orla Gallagher, Julia Hough and Darren Lath for helping me with all the histology work for without them the project would not have been completed. I would like to thank Fatma Gossiel for teaching me the art of pipetting and other technical skills in doing a proper ELISA analysis. I would like to thank Holly Evans for all the help in the μCT work and for teaching me MS Excel. I would like to thank Dr. Allan Williams for teaching me multiphoton techniques and the analysis. I would like to thank Dr. Ishtiaq Rehman who was with me as a constant source of support and guidance throughout this M.Sc., project.

I would also like to thank Dr. Martin Nicklin who was there at all times throughout the course.

## SUMMARY

**Introduction:** With the increasing use of preclinical animal models in the field of prostate cancer bone metastasis research, the development of an ideal animal model which represents the human disease condition is necessary for better understanding of the disease pathogenesis and development of therapeutic interventions. The major problem dealt by researchers is the development of animal model which metastasize to bones. Hence we aimed at developing NOD/SCID mice as model for prostate cancer bone metastasis studies.

**Materials and Methods:** In a view to characterise the mice model we determined the age related changes in the bone turnover in the male and female NOD/SCID mice. We assessed the changes in the tibial and vertebral micro architecture by μCT, changes in the concentration of bone formation and resorption markers by ELISA analysis and changes in the cellular composition by static histomorphometry between 5 and 14 weeks.

In the second part, we studied the early events of PC3-GFP-Tib3 tumour cell homing and colonisation in 5 weeks male NOD/SCID mice using multiphoton microscopy.

**Results** NOD/SCID mice of showed increase in both trabecular and cortical bone volume with increase in age between 5 and 14 weeks. A decrease in the serum bone marker for bone formation and resorption was seen with reduction in osteoblast and osteoclast parameters were observed with increasing age. Further the animals were in a phase of bone growth (modelling) with a steady decline in growth rates with increase in age. Following intracardiac injection more cells were able to demonstrate GFP positive cells in the bone marrow of tibia for up to 1 week.

**Conclusion:** In NOD/SCID mice despite increase in bone growth, there is a steady decrease in the growth rate with increase in age of the mice from 5 to 14 weeks as they were attaining skeletal maturity. We observed high bone turnover rates in 5 weeks mice compared to the rest of the study group. Following intracardiac injection PC3-GFP-Tib3 cells home to the bone marrow and can be seen up to 1 week post injection.

# CONTENTS

## TABLE OF FIGURES

## LIST OF TABLES

## ABBREVIATION

| | |
|---|---|
| % BV | Percentage Bone Volume |
| μ CT | Micro Computed Tomography |
| BMD | Bone Mineral Density |
| BMP | Bone Morphogenetic Protein |
| BV | Bone Volume |
| CAM | Cell Adhesion Molecules |
| Ct.V | Cortical Volume |
| CTX | Carboxy Terminal Telopeptide |
| CXCL12 | Chemokine (C-X-C motif) ligand 12 |
| CXCR4 | Chemokine, CXC Motif, Receptor 4 |
| DC-STAMP | Dendritic Cell – Specific Transmembrane Protein |
| DMEM | Dulbeco's Modified Eagle's medium |
| DPX | p-Xylenebispyridinium Bromide |
| Ec.Pm | Endocortical Perimeter |
| EDTA | Ethylenediaminetetracetic Acid |
| EGF | Epidermal Growth Factor |
| EIA | Enzyme Immunoassay |
| ELISA | Enzyme-Linked Immunosorbent Assay |
| FGF | Fibroblast Growth Factor |
| GEM | Genetically Engineered Mice |
| GFP | Green Fluorescent Protein |
| $H_2SO_4$ | Sulphuric Acid |
| HBME | Human Bone Marrow Endothelium |
| HCl | Hydrochloric Acid |
| IGF | Insulin-Like Growth Factors |
| IGF-BP3 | IGF Binding Protein 3 |
| IGFIR | IGF-I Receptor |
| IL | Interleukin |
| IMS | Industrial Methylated Spirit |
| LFA | Leukocyte Functional Antigen |
| M-CSF | Macrophage Colony Stimulating Factor |
| MIP | Macrophage Inflammatory Protein-1 |
| MT1-MMP | Membrane type-1 metalloproteinase |
| N.Ob.Pm | Percentage Trabecular bone surface covered by Osteoblast |
| N.Oc.Pm | Percentage Trabecular bone surface covered by Osteoclast |
| NF-ĸB | Nuclear Factor Kappa B |
| NOD/SCID | Non-Obese Diabetic Severe Combined Immune Deficient mice |
| NPT | Sodium Dependant Phosphate Transporters |

| | |
|---|---|
| OB | Osteoblast |
| Ob.Pm | Osteoblast Perimeter |
| Ob.Pm/Ec.Pm % | Percentage Endocortical surface covered by Osteoblast |
| OC | Osteoclast |
| Oc.Pm | Osteoclast Perimeter |
| Oc.Pm/Ec.Pm % | Percentage Endocortical surface covered by Osteoclast |
| OCT | Optimal Cutting Temperature |
| ODF | Osteoclast Differentiation Factor |
| OPG | Osteoprotegerin |
| P1NP | Procollagen 1 N-Terminal Peptide |
| PBS | Phosphate Buffered Saline |
| PDGF | Platelet Derived Growth Factor |
| PSA | Prostate Specific Antigen |
| PTH | Parathyroid Hormone |
| PTHrP | Parathyroid Hormone Related Protein |
| RANK | Receptor For Activation Of Nuclear Factor Kappa B |
| RANKL | RANK Ligand |
| ROI | Region Of Interest |
| RT | Room Temperature |
| RT | Room Temperature |
| SCID | Severe Combined Immune Deficient |
| SDF | Stromal Derived Factor |
| SMI | Structural Model Index |
| sRANKL | Soluble RANKL |
| Tb.N | Trabecular Number |
| Tb.Pf | Trabecular Pattern Factor |
| Tb.Pm | Trabecular Bone Perimeter |
| Tb.Th | Trabecular Thickness |
| TGF-B | Transforming Growth Factor B |
| TMB | Tetramethylbenzidine |
| TRAMP | Transgenic Adenocarcinoma In Mouse Prostate |
| TRAP | Tartrate Resistant Acid Phosphatase |
| uPA | Urokinase-Type Plasminogen Activator |
| uPA-R | Urokinase-Type Plasminogen Activator Receptor |
| VCAM | Vascular Cell Adhesion Molecules |
| VEGF | Vascular Endothelial Growth Factor |

# CHAPTER 1 INTRODUCTION

## 1.1 BONE METASTASIS

Despite imminent advancements in the field of cancer research, treatment for cancer and its complications remains unconquered. A successful strategy in treating cancer depends not only on the treatment of the primary tumour but also on the treatment in the prevention and eradication of the cancer spread to the different anatomical sites. This spread of tumor cells from the primary tumour to distant sites is described as 'Metastasis'. The mechanism behind this phenomenon is extremely complex and still remains poorly understood. Previous studies have demonstrated a definite metastatic pattern associated with different cancers (Hart 1982). For example breast and prostate cancer have a high propensity to bone metastasis while colon cancer preferentially metastasizes to the lungs and liver. This pattern of organ and site specificity in tumour metastatic behaviour depends on the communication between the compatible metastatic tumour cell and a premetastatic niche i.e., a compatible organ microenvironment (Ribatti *et al.* 2006). Various factors have been attributed to intercede this organ specificity which includes tumour specific chemotactic and growth factors; physical and mechanical properties of metastatic tumour cell; and organ microenvironment. The latter includes cell surface characteristics and adhesion properties between the tumour cell and the organ microenvironment (Ribatti *et al.* 2006). However, researchers have also explained the role of the anatomical location of the primary tumour and the pattern of venous and lymphatic drainage to a preferential location (Takanori *et al* 1994). The site specificity of tumour cell to metastasize to particular organs was described by Dr. Stephen Paget in his '*Seed and Soil Hypothesis*' 1889 (Paget 1889). Studies have established the role of bone released growth factors and chemokines in the facilitation of the tumour cell homing and colonisation in the bone. However what remains largely unknown is the complex interaction and the molecular theory behind these cell to cell interactions.

### 1.1.1 PROSTATE CANCER AND BONE METASTASIS

Prostate cancer is the second most common cause of cancer related death and the most common cancer in men after lung cancer, affecting 1 in 14 men in their life time in the UK. According to the Office for National Statistics, 2009 prostate cancer was responsible for the death of around 10,239 men in

the UK and around 27,000 in the U.S (Taichman *et al* 2007). Prostate cancer is frequent in Northern Europe and Scandinavia with an increase in the incidence seen after the age of 55. According to Cancer Research UK more than 60% of cases diagnosed in men are over 70 years of age. The most common type of prostate cancer is the adenocarcinoma of the prostate. It has been shown that approximately 70% of men have prostate cancer at the time of their death, when examined by autopsy (Taichman *et al* 2007). Metastasis to bone and lymph nodes are a frequent complication of prostate cancer. Bone metastases in prostate cancer can cause osteosclerotic or an osteolytic phenotype. The basic pathogenesis of metastatic growth in prostate cancer is the disruption of normal regulated bone remodeling mechanisms. This results in an imbalance between osteoclast induced bone resorption to inapt bone formation.

### 1.1.1 EPIDEMIOLOGY OF BONE METASTASIS

It has been estimated that around 350,000 people die a year in the U.S with bone metastasis (Roodman 2004). The incidence was forecasted at around 225,174 in 2008 by Cancer Market Trends 2008-2012, with prostate and breast cancer contributing a significant proportion of around 65-70%.

### 1.1.2 PATHOPHYSIOLOGY AND CLINICAL MANIFESTATION

Skeletal metastasis is the most life threatening complication of prostate cancer. Clinical signs of malignant bone disease are observed in almost 85% of prostate cancer patients dying of the disease and its complications (Carlin and Andriole 2000). Bone metastases in prostate cancer have a high propensity for the spine, pelvis and the ribs (Eaton and Coleman 2003). Advanced bone disease causes severe infringement in the patients' quality of life, with significant morbidity and mortality. Bone metastases cause intractable pain which may be constant or intermittent. Metastasis with osteolytic lesions results in progressive bone weakening; this often results in pathological bone fractures. Vertebral metastases results in pathological fractures leading to collapse and compression of regions of the spinal cord resulting in partial to complete paralysis. Furthermore, life threatening complications of bone metastasis includes hypercalcaemia; and marrow suppression often resulting in causing cardiac arrhythmias, renal failure and total bone marrow failure.

## 1.2 BIOLOGY OF BONE REMODELING

Bone is a living tissue composed of hard mineralized matrices which is in a state of constant remodeling. Bone remodeling serves several physiological functions which include preserving structural integrity, strength against mechanical stress and building a congenial environment for haematopoiesis (Kollet *et al* 2007, Abkowitz *et al* 2003). Bone remodeling is a dynamic process which involves active osteoclastic bone resorption forming resorption pits (lacunae) followed by a reversal phase (Fig 1). The phase of bone formation ensues where the osteoblast forms and deposits osteoids resulting in new bone formation. This bone remodeling is a strictly regulated process with a balance existing between the bone loss and new bone formation. (Eaton and Coleman 2003).

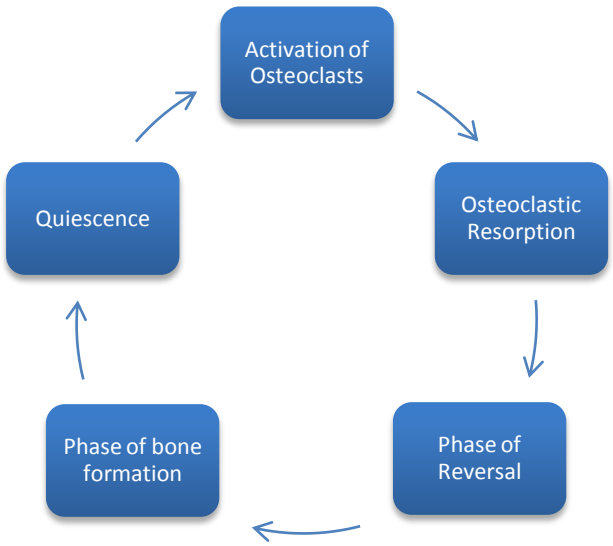


**Figure 1**: Phases in Bone Remodeling.

## 1.2.1 COUPLED BONE REMODELING

### 1.2.1.1 PHASE OF BONE RESORPTION & OSTEOCLASTOGENESIS

Osteoclasts are derivatives of hematopoietic stem cells of the monocyte - macrophage lineage and the principal instrumental involved in bone resorption. The phase of bone resorption is a complex multistep process which begins with the recruitment of the hematopoietic progenitor cells to the site of active bone remodeling. Following the recruitment phase is the differentiation and proliferation of the committed pre-osteoclasts which involves a cell to cell interaction of the osteoclast progenitors with stromal cells/osteoblasts (Udagawa 2003). The next step involves the activation of the pre-osteoclasts into mature functionally active osteoclast which resorb the bone (Hill 1998). Receptor for activation of nuclear factor kappa B (NF-ĸB) ligand (RANKL) and macrophage colony stimulating factor (M-CSF) are two important molecules involved in the maturation, proliferation and survival of the osteoclast. RANKL, also termed as osteoclast differentiation factor (ODF) is expressed by osteoblasts and the stromal cells and binds with RANK expressed on the osteoclast surface and their precursor leading to osteoclastogenesis. Recent reports suggest the involvement of the chemokine molecules CXCL12, macrophage inflammatory protein-1α (MIP-1α/CCL3) and monocyte chemoattaracant protein (MCP-3/CCL7) involved in osteoclast maturation and activation (Gronthos *et al* 2007). In 2005, Vignery suggested a possible mechanism for the formation of multinucleated osteoclasts. Following activation by RANKL the osteoclasts express dendritic cell – specific transmembrane protein (DC-STAMP) on their cell surface which fuses with DC-STAMP negative osteoclast cells to form multinucleated osteoclasts (Vignery 2005).

In 1992 Meikle *et al* suggested the role of osteoblast cells in promoting osteoclastic bone resorption by producing Matrix metalloproteinases (MMPs) like collagenase, stromelysin and gelatinase B to remove the unmineralised osteoid layer and exposing the underling bone surface to allow osteoclast attachment. The adhesion of the osteoclast to the bone surface is aided by the integrin superfamily of adhesion receptors (Hill 1998). Next the activated osteoclast digests the bone minerals forming resorption pit. This occurs in two steps, firstly hydrogen ions digests the hydroxyapatite or the mineralized matrices of the bone and secondly the organic component is broken-down by the proteolytic enzymes produced by the osteoclast including cathepsin B, L, K and the MMPs produced by the osteoclast (Hill *et al* 1994).

### 1.2.1.2 REVERSAL PHASE

Following osteoclastic bone resorption a reversal phase ensues with the gradually apoptotic death of the osteoclasts thus impeding resorptive activity. The accumulation of calcium ion and transforming growth factor β (TGF-β) released from the resorption lacunae has been attributed to the inactivation the osteoclastic activity (Zaide *et al.*, 1990; Pfeilschifter *et al.*, 1990)

### 1.2.1.3 BONE FORMATION PHASE

The accumulation of growth factors released due to resorption activity results in a complete end to osteoclastic activity. Next osteoblasts and their precursors are recruited to the resorption pit. Growth factors like TGF-β, Insulin like growth factor (IGF) I and II, fibroblast growth factor (FGF), bone morphogenetic protein (BMP) and platelet derived growth factor (PDGF) are involved in the proliferation, differentiation and maturation of the osteoblasts (Hill 1998). Osteoblasts are derived from osteo-chondro-progenitor cells which is a common progenitor lineage for both osteoblasts and chondrocytes, derived from primitive mesenchymal stem cells (Hartmann 2006). Recent studies suggest the involvement of specific signalling pathways and transcription factors like wnt/β-catenin signalling pathway upregulation and activation of transcription factors like *Runx2, ATF4* and *osterix* that directs the differentiation of the common osteo-chondro-progenitor lineage into committed osteoblasts lineage (Krane 2005 and Hartmann 2006). Committed osteoblasts lay down new bone matrix in the resorption pit which is then mineralised. Some osteoblast goes on to be quiescent bone lining cells (Hill 1998). Fig 2 illustrated the cellular and molecular events that occur during normal bone remodeling activity.

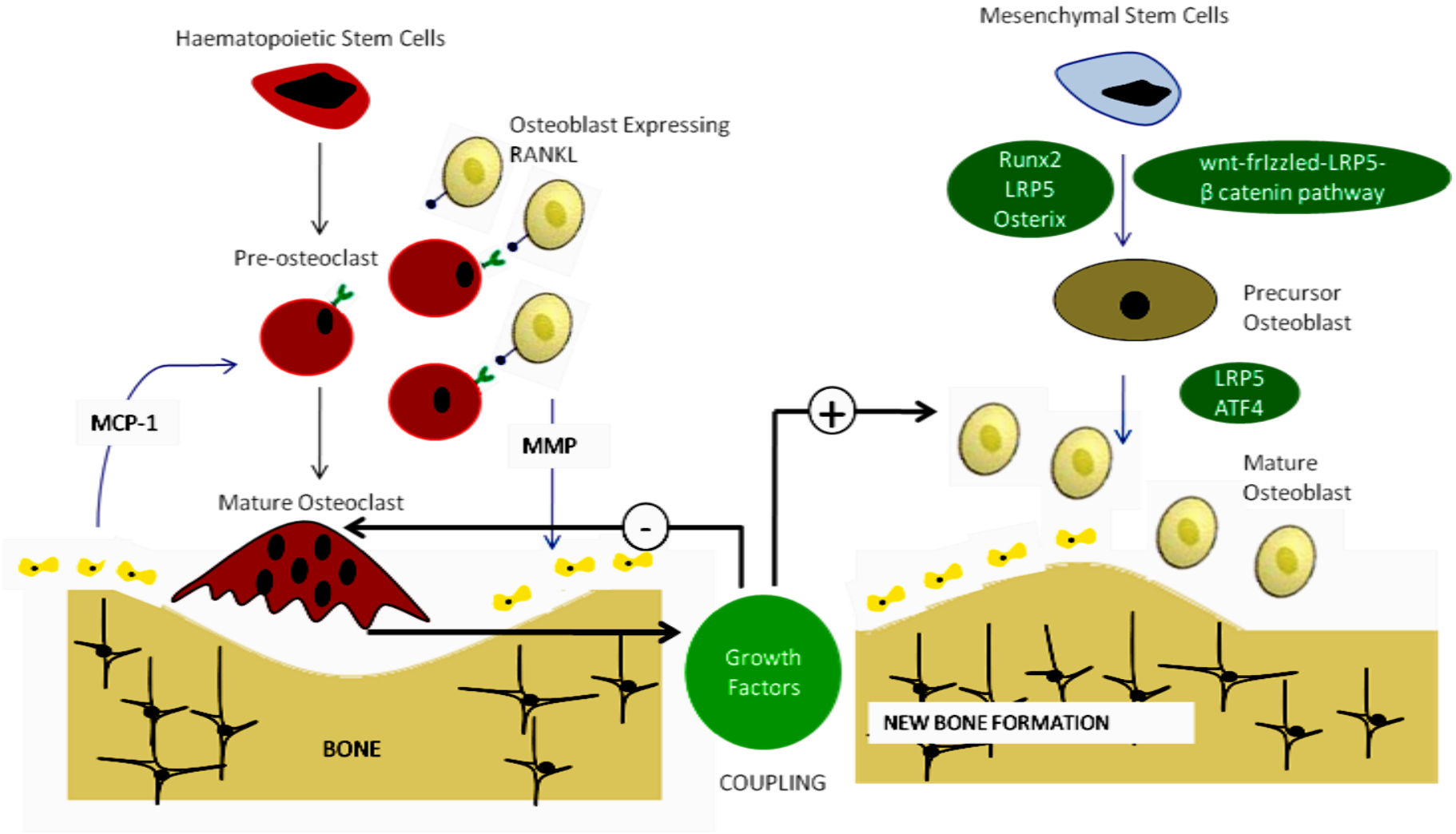


**Figure 2**: Coupled Bone Remodeling
Molecular mechanism of coupled bone remodelling.

## 1.3 TUMOUR BIOLOGY OF BONE METASTASIS

The role of bone turnover in bone metastasis has been widely established. However this interaction doesn't exist between all tumour cell types as only cancer such as breast, prostate, myeloma and lung cancer has a high propensity to metastasize to bone. These tumour cells express exceptional biological properties which aid their development and favours metastases to bone (Yoneda and Hiraga 2005). The two important characteristic features of metastases is the development or the presence of a congenial soil (bone microenvironment) and the release of factors that aids the migration, development and proliferation of the tumor cell. This in turn aids in the development of the congenial microenvironment. This vicious cycle is the result of contribution from both arms of the spectrum which helps in tumour development and metastases. For example osteoclastic bone resorption has been attributed to play an important role in aiding bone metastasis in breast cancer. Osteoclastic bone resorption results in the release of growth factors like IGF-I and TGFβ and also serves as a source of free calcium [$Ca^{2+}$] and phosphate [$PO_4$]. TGFβ and $Ca^{2+}$ ion via TGFβ receptor I and II and calcium sensing receptors respectively results in production of parathyroid hormone related protein (PTH-rP). This activates osteoblasts up regulating RANKL expression which results in the maturation of pre-osteoclast into large multinucleated osteoclasts causing bone resorption. IGF-I and $PO_4$ through IGF-I receptor (IGFIR) and sodium dependant phosphate transporters (NPT) respectively in the tumour cells aid in the proliferation, differentiation, migration and survival of the tumor cell (Yoneda and Hiraga 2005). Likewise previous studies have suggested the involvement of unidentified factors released by osteoblast in promoting prostate cancer cell proliferation (Chackal-Roy 1989 and Gleave *et al* 1991). Furthermore evidence suggest the release of growth factors like BMPs, TGFβ, IGF, PDGF, vascular endothelial growth factor (VEGF), urokinase-type plasminogen activator (uPA) and prostate-specific antigen (PSA) by prostate cancer cells results in an osteoblastogenic response (Logothetis and Lin 2005).

### 1.3.1 PROSTATE CANCER CELL AND BONE METASTASIS

In humans, bone metastasis in prostate cancer mainly exhibits an osteoblastic phenotype. This is unlike breast cancer and multiple myeloma which are primarily osteolytic in nature. This osteoblastic pattern of bone metastasis is due to the disruption in the balance of bone remodeling. The release of

osteogenic growth factors from the prostate cancer cells drives the balance to a primarily osteoblastic response. However, the initial event appears to be an osteolytic event following which there is a osteoblastic phase which results in the formation and deposition of abnormally woven bones over the lytic areas.

Physiological bone remodeling releases various growth factors and cytokines into the bone microenvironment. Many factors are involved and interact with the growth and development of the prostate cancer cells leading to bone invasion and establish metastatic deposits (Vela *et al* 2006). Chemotactic attraction and organ specific adhesion molecules play a vital part in the initial localisation and homing of the prostate cancer cells from the initial tumour site to the bones. Once in the circulation the effectiveness of the metastatic prostate cancer cell to form distant metastases depends on their ability to adhere to the vascular bed and migrate from the blood vessel to the bone marrow microenvironment (Loberg *et al* 2006). Based on this, the early events of prostate cancer cell metastasis to bone can be divided into several stages.

### 1.3.1. 1 CHEMOTAXIS

The role of collagen I has been extensively studied in prostate cancer cell chemotaxis to bone. Collagen I act as a chemoattractant molecule not only for endothelial cells in bone growth (Palmeiri *et al* 2000) but also in prostate cancer bone metastasis and other tumour cell lines (Hall *et al* 2006 and Mundy *et al* 1981). Collagen I bind with collagen I α2β1 receptors, expressed by the metastatic prostate cancer cells; and this increases the chemotactic potential and increased tumour cell migration to the bone (Hall *et al* 2006). Jacob *et al* in 1999 in *in vitro* experiments demonstrated the role of osteonectin, a product of bone formation synthesised by osteoblasts during physiological remodeling in enhancing cancer cell chemotaxis and invasion. Epidermal growth factor (EGF) was found to induce chemotaxis and metastasis in both *in vitro* and *in vivo* models (Angelucci *et al* 2006; Onganer & Djamgoz *et al* 2007).

The role of the chemokine SDF-1 in the initial adhesion of the prostate cancer cell in human bone has been widely established (Keller *et al* 2001 & Taichman *et al* 2002). SDF-1 binds to CXCR4 expressed by prostate cancer cells and the selective expression of SDF-1 by osteoblast, fibroblast and the

human bone marrow endothelial cells (HBME) cells and not by other vascular endothelial cells, explains the trophism of prostate cancer cells to bone (Imai *et al* 1999).

The role of other chemokines like MCP-1/CCL2 and CXCL16 binding with their receptors CXCR2 and CXCR6 respectively has been reported to be involved in chemotactic attraction and metastases development in prostate and breast cancer (Lu *et al* 2008). However reported, what largely remains unknown are the functional mechanisms and molecular interactions of these chemokine mediated pathway which could serve as potential target molecules for drug development to inhibit tumour cell invasion and metastatic spread.

#### 1.3.1.2 ADHESION WITH THE BONE MICRO ENVIRONMENT

The cell to cell interaction between the cancer cell and tumour microenvironment is mediated by adhesion molecules present in the bone and the HBME. The organ specificity in tumour metastasis depends on the selective expression of cell adhesion molecules (CAMs) by the organ (Keller *et al* 2001). Several adhesion molecules have been demonstrated to play an active role in prostate tumour cell adhesion to the bone microenvironment. Adhesion molecules like galectin-3, vascular adhesion molecule (VCAM), CD11α-L, CD18β2 and leukocyte functional antigen-1 (LFA-1) promoted initial adhesion of the prostate cancer cells to the HBME (Cooper and Pienta 2000). Cooper and Pienta have also suggested the role of vascular adhesion molecules in the initial attraction of the tumour cells by the HBME and their function in the extravasation of the tumour cells into the bone microenvironment. Recently another adhesion molecule cadherin-11, involved in the prostate cancer cell metastasis to the bone, has been demonstrated (Chu *et al* 2008).

Once across the HBME, the tumour cells interact with the bone marrow components like collagen-I, osteonectin and the osteoblast. Most of the above mentioned adhesion molecules were described based on *in vitro* assays using cell lines and the tumour formation rates in *in vivo* models by inhibiting these molecules (Koblinski *et al* 2005)

#### 1.3.1.3 TUMOURIGENESIS

Growth factors released during the process of physiological remodelling, especially osteoclastic resorption plays a vital role in the preparation of a pre-metastatic niche suitable for tumour cell colonisation, growth and expansion. Membrane type-1 metalloproteinase (MT1-MMP); produced by tumor cells; helps in matrix degradation and favours tumour cell expansion (Bonfil *et al* 2007b). In addition, they also encourage osteoclastic bone resorption by producing soluble RANKL (sRANKL) which enhances osteoclastogenesis, the effect of which is augmented by the addition of OPG, a decoy receptor for RANKL (Bonfil *et al* 2007a).

IGF not only plays a vital role in prostate cancer cell chemotaxis to bone but also in cell proliferation (Ritchie *et al* 1997). Tumour cells express the IGF receptor which binds the circulating IGF enhancing tumour cell proliferation and survival by the activation of the androgen receptor and the NF-κB signalling pathway, even in the event of androgen deprivation (Bogdanos *et al* 2003). Furthermore tumour cells and osteoblasts both have a more direct role in increasing the IGF bioavailability. Prostate cancer cell produces uPA which binds with uPA receptor (uPA-R) on the osteoblasts and results in a proteolytic activity causing degradation of IGF-binding proteins which is a competitive receptor for IGF compared to IGF receptor expressed by the tumor cells (Bogdanos *et al* 2003).

In 1989, Chackal-Roy *et al* showed TGF-β has an inhibitory role in prostate tumor cell growth whereas later studies demonstrated a low dose of TGF-β having a stimulatory effect on tumor cell survival and proliferation (Sylvie *et al* 1996 and Ritchie *et al* 1997). However, the mechanism in the regulation of tumour cell survival by TGF-β is still not clear.

The role of FGF 8b isoform as a potent mitogen, stimulating tumour cell proliferation, was demonstrated using LnCaP cells in *in vitro* and in *in vivo* models studying the tumor invasion properties into the muscles (Song *et al* 2000). The role of FGF in tumourigenesis in bone is not well established.

### 1.3.2 BONETURNOVER AND TUMOUR CELL COLONISATION

As already described, several factors involved in active bone remodeling play a vital role in the initial prostate cancer cell chemotaxis and adhesion to the bone microenvironment. Recently in 2005,

Schneider *et al* demonstrated that metastatic prostate cancer cell prefers to areas of active bone turnover and dense marrow cellularity. This was demonstrated by using PTH to induce bone turnover and bisphosphonates to inhibit it. Sasaki *et al* in 1995 demonstrated that altering bone turnover by using bisphosphonates, an inhibitor of osteoclastic resorption resulted in less tumor take rate and eventually lower tumor burden and longevity in metastatic breast carcinoma. The bone is in a dynamic state of physiological remodelling releasing growth factors continuously that augments the chemotactic attraction and adhesion for tumour cells and also creates a favourable niche for colonisation and growth. Significant controversy persists with the works of Cross *et al* 2008 that shows PC3 cells are significantly independent over an area of physiological remodeling compared to an extrinsically induced area of high bone turnover (a pre existing osteoclastic niche) in tumour colonisation rates. Moreover the direct action on the tumour cell by PTH and the anti-tumour activity of bisphosphonates were not considered in the former studies. Further in the works of Cross *et al* the bone turnover was altered by castration suggesting this distorted tumour behaviour might be due to altered environmental and hormonal conditions created by castration. Previous studies reported the unusual occurrence of mandibular metastases in rodent models which was attributed to the fact that continued tooth eruption in rodent models provides an area of high turnover making it a niche for tumour homing (Schneider *et al* 2003). In addition increase in tumour take rate in young mice compared to older animals also substantiate that prostate cancer cells prefers areas of high bone turnover as in older mice bone remodeling takes a more steady phase compared to younger mice (Schneider *et al* 2003).

## 1.4 ANIMAL MODELS

The role of active bone turnover and the products of bone remodeling that are involved in increased propensity of prostate cancer metastases to bone have been widely established. However, the molecular mechanism behind this cell to cell interaction remains largely unknown. With development of newer therapeutic strategies and novel disease mechanisms the need for understanding the undeciphered blocks of information becomes mandatory for therapeutic improvisation. Despite the increasing use of human tissues in the field of biomedical research, however stands imperfect without the complete representation of the whole *in vivo* condition with complex multi-cellular interactions (Chaoyong 2004). Animal models have become an obligatory instrument in the hands of the researchers to fill in these gaps

of information. The development of an ideal animal model for the study of bone metastasis in prostate cancer has been a challenge. Researchers have tried different animals and different approaches for tumour cell inoculation from orthoptic implantation to intra-osseous implantation of the tumour cell or human bone implantation into mice to study the bone metastasis of prostate cancer.

### 1.4.1 PROSTATE CANCER ANIMAL MODELS

Presently several different pre-clinical animal models have been developed for studying bone metastasis in different cancer conditions like leukaemia and carcinoma of breast and prostate, of which for prostate cancer majority of them are rodent models. The currently available models are representative of only specific stages of the human disease condition (Thomas *et al* 2003). However till date no single model appears to mimic the human disease condition. Few reasons for this are

- The complexity of the pathobiology of the human prostate cancer and its metastatic pattern is not yet well characterised (Pienta *et al* 2008).
- There are differences in the microscopic and macroscopic anatomy of the prostate gland between humans and animal models (Thomas *et al* 2003).
- The rate of incidence in the development of prostate cancer in animals is significantly low compared to humans and evidence of spontaneous bone metastasis is rare in animals (Thomas *et al* 2003).

Rodent models have been extensively used in prostate cancer pre-clinical research. Despite spontaneous prostate cancer development in rats evidence of bone metastases in spontaneous tumour development models and chemical carcinogenesis models is very rare (Blouin *et al* 2005). Osteoblastic metastases were observed in the Gedolf-Rao model where a Mat-Ly-Lu subline of Dunning R-3327 cells were injected to male Copenhagen rats (Blouin *et al* 2005). Other prostate cancer rats models used include the Lobund wistar and Noble rats (Huss *et al* 2001).

Osteoblastic metastasis with abnormally woven bone is observed in canine models of prostate cancer. Interestingly dogs, like humans has spontaneous prostate cancer incidence observed with increase age with metastasis to bones (Waters *et al* 1998). The large size of dogs aids in uncomplicated tumour cell

imaging. In addition, the development of spontaneous tumour and metastasis has rendered dogs a more suitable model for studying the initial events in the tumour cell interaction with bone. However the cost and maintenance of dog colonies have a profound impact in employing dogs as basic models in pre-clinical animal research.

The development of genetically engineered mouse (GEM) models has revolutionised the field of cancer research in developing pre-clinical animal models. Increase in the use of GEMs and human cell lines like PC3, DU145 and LnCaP is being observed (Pienta *et al* 2008). The transgenic adenocarcinoma of the mouse prostate (TRAMP) model and the LADY tumour model (where the small T antigen expression is genetically removed) was a breakthrough in prostate cancer pre-clinical research. The TRAMP model exhibits a highly metastatic pattern of tumour development while the LADY model shows a locally aggressive tumour development with no metastasis (Lamb and Zhang 2005). The PTEN deletion of phosphates and tensin homologue in chromosome 10 knockout mice are widely used in the area of chemoprevention research for prostate cancer (Kazunori *et al* 2009).

According to a recent review, Weerden and Romijn in 2000 described 25 established xenograft models in prostate cancer research. Immunodeficient animals have paved a great deal of opening in the development of xenograft models as the primary problem with tumour cell inoculation is graft rejection. Several xenograft animal models have been described from athymic nude mice to severe combined Immunodeficient (SCID) mice (Lamb and Zhang 2005). Further improvisation developed in this area with the development of NOD/SCID strain by Schultz et al in 1995 by crossing the Non-obese diabetic (NOD) and the SCID strain which developed a strain completely devoid of T, B and natural killer cell which resulted in enhanced tumour take rate; however no evidence of spontaneous bone metastases were observed. Several models have been developed in the NOD/SCID strain using human prostate derived xenograft cell lines which include PC3, LnCaP and DU-145.

### 1.4.2 NOD/SCID MICE

Recently, in 2002 a group of scientist used the NOD/SCID mice for development of a new animal model for prostate cancer studies. Interestingly this mouse model had more metastatic sites compared to the previously described animal models (Bastide *et al* 2002). PC3 and DU145 cell lines were

used for the study. Both subcutaneous and orthoptic implantation of tumour cells were preformed with 80% metastases overall in both these cell lines. Tumour metastasis was observed in multiple sites including lymph nodes, lungs, liver, pancreas, spleen, kidney adrenal and diaphragm. However no evidence of bone metastasis was described and the reason for this unusual pattern of the tumour cell behaviour ignoring the bone for tumour homing and metastatic spread however remains unknown (Bastide *et al* 2002). Despite its relative efficiency over other available mice models in developing orthoptic and multiple visceral metastases, the lack of its ability to develop bone metastasis has led to a state of under utilization of this NOD/SCID mice model in 'bone metastasis in prostate cancer' studies.

### 1.4.3 PC3-GFP-TIB3

PC3-GFP-Tib3 cells were developed by Cross *et al* 2008 in the Section of Oncology, at The University of Sheffield Medical School, UK. Initially PC3-GFP cells were extracted from subcutaneous tumour sites in athymic nude mice and were then cultured *in vitro*. These subcutaneously tumourigenic cells were then used for intra tibial inoculation where intra tibial tumour developed in 2/6 animals (Cross *et al* 2008). Tumour development in the tibia was visualised using fluorescent imaging (Fig. 5). PC3-GFP cells were isolated from the intra-osseous tumour sites were cultured *in vitro* and were again re-implanted into the tibia. The tumour take rate was 100% and this highly tumourigenic cells were termed as PC3-GFP-Tib cells. The term PC3-GFP-Tib3 means that the tumour cells have been passaged *in vivo* three times and expanded *in vitro* (as shown in Fig. 3). The PC3-GFP cells offer the advantage of studying the tumour interaction with the host environment in a three dimensional temporo-spatial orientation using the appropriate imaging technique. Fig 4 show the fluorescent microscopic image of PC3-GFP-Tib3 cells.

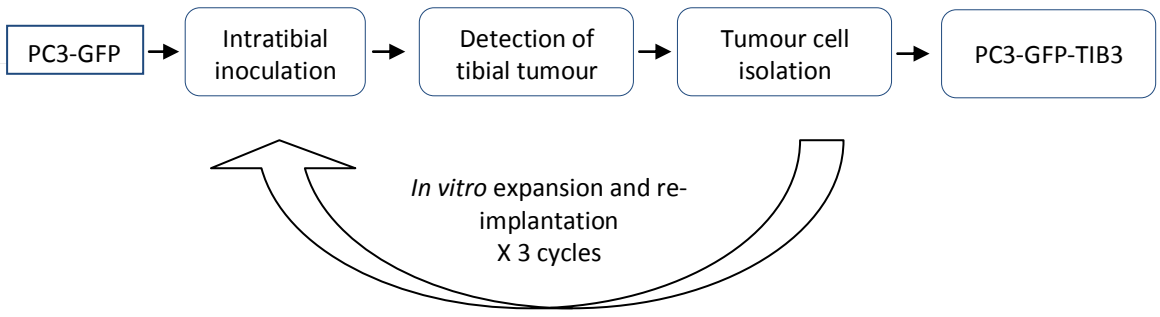


**Figure 3:** Development of metastatic variant PC3-GFP-Tib3 subline (Cross *et al* 2008).

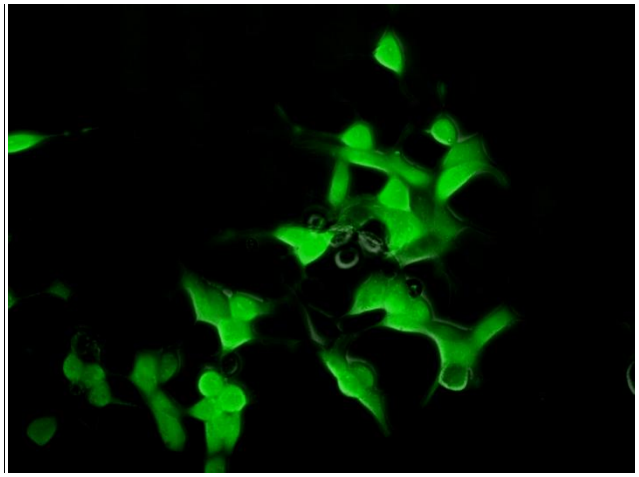

**Figure 4:** *In vitro* PC3-GFP cell colony under fluorescent microscope**.**
*Photograph: Courtesy Anne Fowles.*

**A**. Visualisation of metastatic growth in the lower limb of mice with PC3-GFP cells under fluorescent light

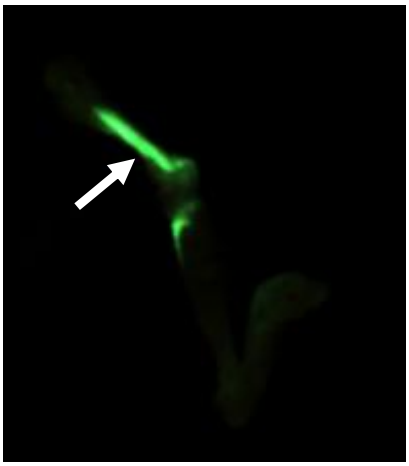

**B**. Dissected tibia and femur showing metastatic growth under fluorescent light.

**Figure 5 :** Visualization of metastatic growth in mice injected with GFP labelled PC3 cells
*Photographs: Courtesy Anne Fowles.*

## 1.5 AIMS AND HYPOTHESIS

The increasing use of pre-clinical mice models in the field of prostate cancer bone metastasis may help researchers understand tumour cell behavioural and pattering with the use of the most appropriate xenograft cell lines (Pienta *et al* 2008). These findings may lead to a better understanding of the human disease. We hypothesised that bone turnover decreases with increase in age in NOD/SCID mice and PC3-GFP-Tib3 cells will colonise to specific areas in the bone in NOD/SCID mice following intra cardiac injection.

Our objectives are 1. To determine the age related changes in bone turnover in NOD/SCID mouse strain 2. To study the early events of tumour cell homing and colonisation and determine the behavioural pattern of the PC3-GFP-Tib3 cell line in the bone microenvironment of the NOD/SCID strain when administered by intracardiac inoculation.

# CHAPTER 2 MATERIALS AND METHODS

## 2.1 CELL CULTURE

PC3-GFP-Tib3 cells were provided by Dr. Colby Eaton, University of Sheffield, UK. Cells were maintained at 37ºC in Dulbeco's Modified Eagle's medium (DMEM) with Glutamax™ II, Invitrogen Corp., (Catalogue No. 61965-026) supplemented with 10% (vol/vol) foetal calf serum (AutogenBioclear), Pen-strep and fungizone in a T25 Nunclon flask in a 5% $CO_2$ humidified incubator.

## 2.2 ANIMAL MODEL

Nomenclature: NOD/NCrCrl- $Prkdc^{Scid}$

NOD/SCID mice were purchased from Charles River laboratories, France and were housed and bred in The University of Sheffield Animal facilities. Animal works were approved by the local ethical committee and UK Home Office Regulation.

## 2.3 EXPERIMENTAL PROTOCOL FOR THE LONGITUDINAL STUDY

For the initial longitudinal study 70 mice (35 male + 35 female) in groups of 5 between age groups 5-14 wks at 7 different time points were bred and housed. The schematic representation of the experimental design is given in Fig 6. All animals were injected with intra peritoneal calcein injection (30mg/kg) in 0.2% sodium bicarbonate at day 6 and day 2 before sacrifice. The mice were starved 6 hrs prior sacrifice as circadian rhythm and food intake affects the levels of osteocalcin and carboxy terminal telopeptide of type I collagen (CTX) assay. The mice were anaesthetized by inhalational isoflurane and intra cardiac blood samples collected and the animals killed by cervical dislocation while they were still anaesthetized.

The blood samples were centrifuged at 3000 RPM, 4°C for 10 minutes and serum samples obtained. They were made into 25µl aliquots and frozen at -80°C for later analysis. After the death of the animal the left tibia & femur and lumbar vertebrae $L_1$, $L_3$ and $L_4$ were dissected free of soft tissues and preserved in 10% formalin and the right tibia & femur, vertebrae $L_2$ were stored in 70% ethanol until further analysis. Only the left tibiae and the L1 lumbar vertebrae stored in 10% formalin were used analysed for the current study and the rest of the samples were preserved for future studies.

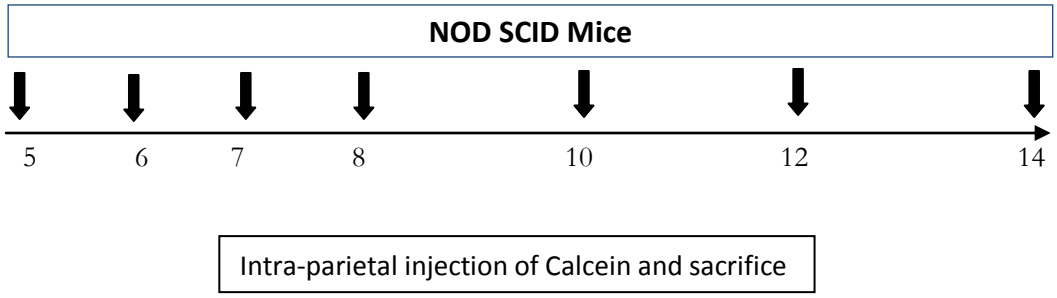


**Figure 6:** Schematic representation of the Experimental Design for Phase I

## 2.4 PC3-GFP-TIB3 CELL IN VIVO COLONISATION STUDY

In a second study 15 NOD/SCID male mice aged 5 weeks were purchased and bred in the University of Sheffield Animal Facilities. The mice were batched in groups of 5 where 1 animal of each group served as the control and the other 4 animals were inoculated by intracardiac injection of PC3-GFP-Tib3 cells. All animals were adequately anesthetized by inhalational isoflurane before the procedure. PC3-GFP-Tib3 cells ($1x10^6$ cells in 1ml) were injected into the left ventricle of the animal and the animals were allowed to recover in an incubator for approximately 20 min. The post procedure was uneventful and all the mice tolerated the procedure well and survived. The time of tumour cell inoculation was counted as 0 hr and sacrifices were done accordingly from this time point. Animals were scarified in batches after 18hrs, 48hrs and 1 week respectively. Tibiae and femura from both the limbs and the lumbar vertebrae were dissected, stripped of their soft tissues and then stored in liquid nitrogen and later transferred to storage under -80°C and until analysis was performed using a multiphoton microscope. A detailed schematic representation of the experimental design for phase II is shown in Fig 7.

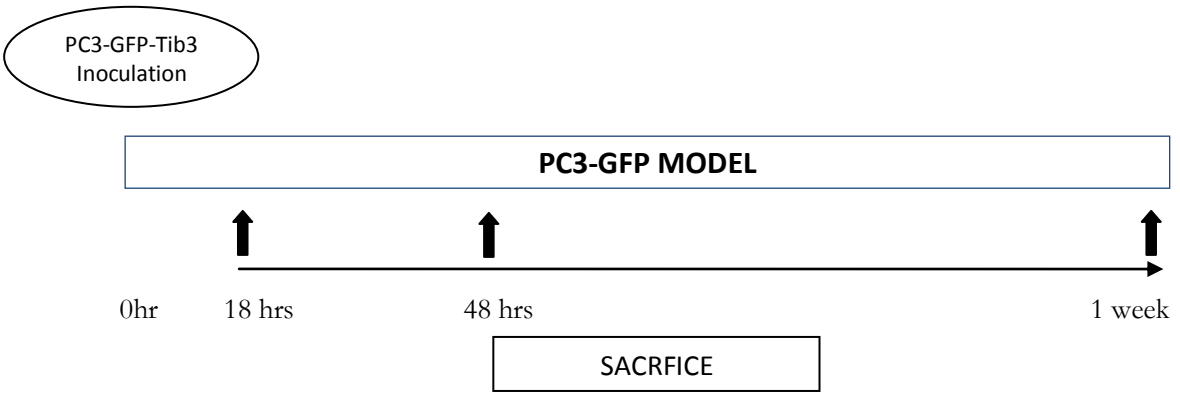


**Figure 7:** Schematic representation of the experimental design for phase II study

## 2.5 MICRO COMPUTED TOMOGRAPHY IMAGING AND ANALYSIS

### 2.5.1 IMAGING

SKYSCAN 1172 DESKTOP X-RAY MICROTOMOGRAPH

μCT analysis was performed using SkyScan 1172 Desktop X-ray tomography scanner manufactured by SkyScan N.V. Aartsalaar, Belgium for complete quantitative analysis of the trabecular and cortical bone changes on the left tibia and the first lumbar vertebrae ($L_1$) prior to decalcification for histology. For a complete quantitative analysis of the bone changes the following parameters were analysed: trabecular bone volume (BV), trabecular thickness (Tb. Th, μm), trabecular number (Tb. N, per $mm^3$), percentage bone volume (%BV), cortical volume (Ct.V), Sructural model Index (SMI), trabecular pattern factor (Tb. pf) and bone density ($mg/cm^2$). The left tibia samples are preserved and fixed in 10% formalin solution until μCT was performed. The specimen is folded onto a household cling film to prevent drying of the specimen and placed upright inside the specimen chamber of the scanner. The proximal tibial metaphysis is scanned using a medium sized camera with a resolution of 2000 X 1048, a 0.5mm aluminium filter and scanned for a pixel size of 4.3μm for every 0.7° rotation for 180 °. The scan took approximately 11 min for each bone. The software used for the purpose of scanning is SkyScan 1172 software version 1.5 supplied by the manufacturer. The scanned images were stored in TIF format.

Similarly Lumbar vertebrae ($L_1$) were scanned using the same method and the same settings. Because of the asymmetrical nature of the vertebrae bone a 360° rotation was done with a view to reduce the asymmetrical artefacts during the scanning.

### 2.5.2 RECONSTRUCTION AND ANALYSIS

**Reconstruction**

Reconstruction of the scanned images was done using NRecon ver. 1.6.1.1 software within a dynamic range of 0 to 0.16 and a ring artefact reduction factor of 1% to minimize the ring artefacts of the scan.

**Analysis**

Analysis of the reconstructed images was done using CT Analyser (CTAn) version 1.7.0.5 for trabecular and cortical parameters in the left tibiae and vertebrae. Analysis was done on a fixed area of the proximal tibial metaphysis which is at a fixed distance from the distal break in the growth plate of the proximal end of the tibia. This break in the distal growth plate of the proximal tibia was chosen as the reference point and standardized for the analysis of both the trabecular and cortical parameters. The region of interest (ROI) was chosen at a fixed distance from this reference point for 1mm in length. For trabecular analysis of tibia, the ROI is chosen at a distance of 0.2mm from the reference point, hence the offset was fixed at -1.202 mm (as the tibia is upright in position) and a fixed area of the metaphysis extending for 1mm was analyzed (Fig. 8 A, B). The gray scale index for the binary images of the ROI is limited to 90-255 for trabecular bone analysis. In the case of cortical analysis, as the differentiation of cortical and trabecular bone is quite ambiguous near the growth plate due to highly porous cortical bone in young mice, an offset value of -464 which corresponds to a distance of 1.999mm from the reference point was chosen for the ROI, which is binarised and analyzed with a threshold of 100 in the gray scale index (Fig. 8 C, D).

Analysis of trabecular bone in the vertebrae was done choosing a fixed volume cylinder of 0.63 diameter inside the body of the vertebrae. The reference point was the break in the lower growth plate of the vertebrae. An offset of 47, which corresponds to 0.2mm, was taken and analysis was done for a region extending for 1.0mm from this offset. The binarised image were analysed setting up a threshold value for trabecular bone between 90-225 and the results obtained in the form of a Microsoft Excel spread sheet.

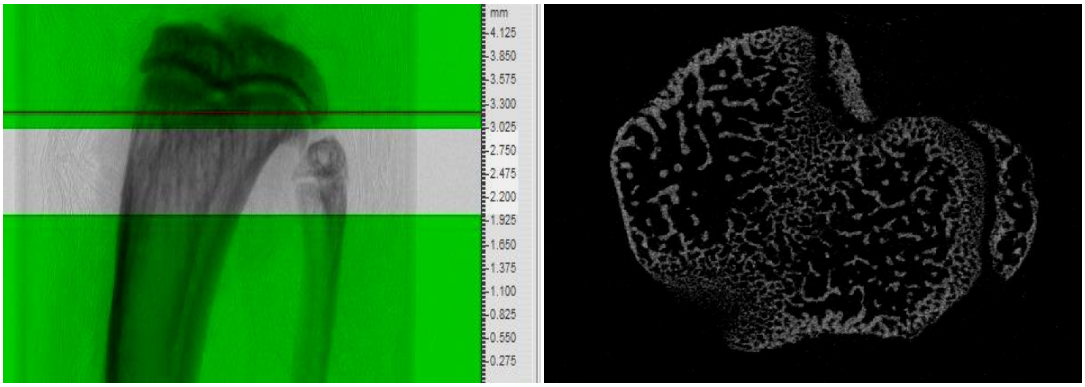


**A.** ROI for trabecular bone analysis with an offset of 0.2mm and height 1mm

**B.** Reference point chosen is the break in the distal growth plate of the proximal tibial metaphysis.

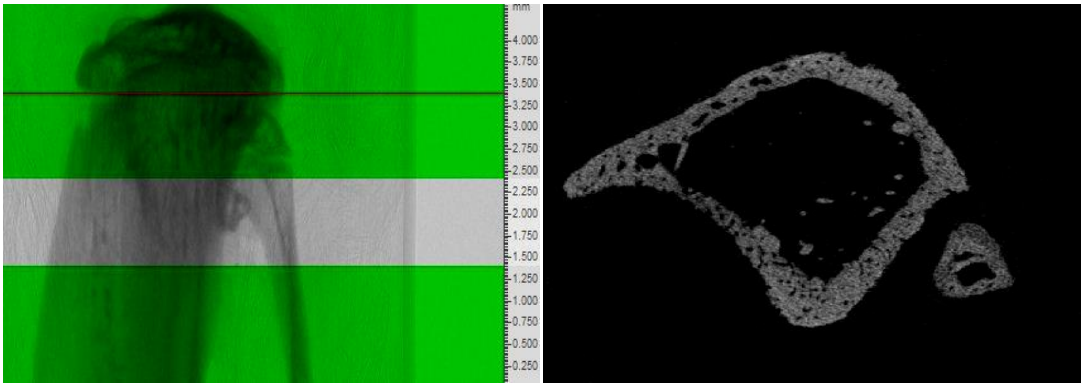


**C.** ROI for cortical bone analysis with an offset of 1.999mm and a height 1mm.

**D.** Cross section of proximal tibia at the level of ROI showing cortical bone.

**Figure 8**: Region of Interest in cortical and trabecular analysis of Left tibia

## 2.6 BIO-MARKERS OF BONE TURNOVER

Enzyme linked Immunosorbent assay (ELISA) was performed to assess the cellular activity and rate of bone turn-over in NOD/SCID mice from 5 to 14 weeks. ELISA was performed for assessing both the bone formation and the bone resorption activity. For Bone formation activity Pro-collagen Type 1 N-Terminal Propeptide (P1NP) and for resorption, CTX Enzyme immune assay (EIA) was done.

### 2.6.1 BONE RESORPTION ELISA

For quantitative determination of bone resorption activity an ELISA that measures bone degradation product CTX of type 1 collagen on serum samples collected from the mice prior to sacrifice was done. The mode of blood collection and obtaining serum samples is described in chapter 2.3. Two RatLaps™ CTX EIA kits (Catalogue No. AC-06F1) were purchased from Immunodiagnostic systems Limited (IDS Ltd), UK as the assays were done in duplicates. RatLaps™ EIA is a competitive assay where polyclonal antibody binds to CTX. The assay procedures were strictly followed according to the manufacturer's protocol. The absorbance was read and analysis was done on an automated plate reader.

Initially pre-incubation of the Biotinylated RatLaps antigen was done by adding 100µL to each well for 30 minutes at room temperature. This pre-incubation resulted in binding the RatLaps antigen to the streptavidin coated microtitre plates. The wells were washed 5 times using 300µL washing solution. 20µL of standards and control solution was added to the appropriate wells. 20µL of the sample solution is pipette into the microtitre wells in duplicates followed by 100µL of primary antibody and allowed for an overnight incubation for 18 hrs at 2-8°C. The plates were washed manually 5 times and 100µL of enzyme conjugate added and incubated (TMB) for 60 minutes at room temperature. The plates were again washed and 100µL of Tetramethylbenzidine added and incubated for 15 minutes in darkness at room temperature. 100µL of stop solution ($H_2SO_4$) was added into all the wells using a multichannel pipette and absorbance was read using an automated plate reader at 450nm with a reference range of 650nm.

### 2.6.2 BONE FORMATION ELISA

Two Rat/Mouse P1NP EIA kits (Catalogue No. AC-33F1) were purchased from Immunodiagnostic systems Limited (IDS Ltd), UK were used for quantitation of bone formation. It is a competitive EIA using polyclonal rabbit anti-PINP antibody coated onto the inner surface of the microtitre wells. The assays were performed following the manufacturer's protocol. The calibrators and controls were reconstituted according to the manufacturer's protocol and 50µL of each added into the appropriate wells in the 96 well plate. 5µL of the each serum samples were added to the appropriate wells in duplicates followed by 45µL of the sample diluents. 50µL of PINP BIOTIN were added to all the wells and incubated for 60 minutes on a shaker at 30°C. The wells were washed three times using 250µL wash solution supplied by the manufacturer. 150µL of the enzyme conjugate was added to all the wells and again incubated for 30 minutes at 30°C. The plate was again washed three times and 150µL of the substrate Tetramethylbenzidine (TMB) added to the wells and incubated for 30 minutes. Finally 50µL of stop solution (HCl) was added and absorbance measured at 450nm with a reference wavelength of 650nm. The change in the colour intensity is inversely proportional to the concentration of the PINP. The calibrators, controls, PINP biotin, enzyme conjugate, TMB and stop solution were supplied by the manufacturer along with the kit.

For all the assays, absorbance was read by SpectraMax M5$^e$ automated plate reader manufactured by *Molecular Devices* and analysis done using the software SoftMax Pro ver 5.2.

## 2.7 BONE HISTOLOGY

### 2.7.1 DECALCIFICATION

Decalcification of the left tibia was done at room temperature using Ethylenediaminetetracetic Acid (EDTA) for a time period of 4 weeks. Neutral EDTA (pH 7) solution was prepared by dissolving 250mg EDTA (disodium salt) in 1750ml distilled water and the resulting solution was neutralised by adding 25mg sodium hydroxide and the final solution was stored at room temperature. The bone samples were put in a volume of EDTA approximately 20 times the volume of the bone sample. EDTA solution was changed once a week for four weeks. On completion of decalcification the bone tissues were loaded on to labelled tissue cassettes and washed in running tap water for 60 minutes to remove EDTA.

### 2.7.2 TISSUE PROCESSING AND WAX EMBEDDING

Decalcified bone tissues were processed using an automated Leica TP1020 carousel tissue processor. In the processor the bone samples were dehydrated, cleared and infiltrated with paraffin wax. The dehydrating fluids used were serial concentration of ethyl alcohol and the clarifying fluid used was xylene and the samples were infiltrated with paraffin wax.

The processed bone tissue samples were placed in metal moulds and embedded adding fresh paraffin wax in solution. The bone samples were positioned diagonally in the stainless steel mould for embedding with the crest of tibia and fibula facing down. The wax was allowed to cool down until the block solidified.

### 2.7.3 SECTION CUTTING AND STAINING

Section cutting of the wax embedded specimen was done using a Leica RM2135 rotary microtome set at a 3µm thickness. Initially the specimens were trimmed until the full tibial epiphysis was exposed and 6 serial sections of 3µm in thickness were cut. Chattering of the specimen during cutting was prevented by softening the exposed tissue surface using ice. The cut sections were then transferred to a water bath maintained at 45°C, mounted on Superfrost Plus slides and stored at 4°C.

### 2.7.4 HAEMATOXYLIN AND EOSIN STAINING

#### DEPARAFFINIZATION AND STAINING

For deparaffinization the slides were placed in slide racks for drying. Dry slides were then dipped in 2 staining jars containing xylene in consecutive steps with 5 minutes in each jar. After dewaxing the slide rack was dipped in 4 consecutive staining jars containing two 99%, 95% and 70% Industrial Methylated spirit (IMS) solution with a standing time of 5 min in each jar for removing xylene. After removal of xylene the slides were rehydrated and cleaned of IMS by rinsing them in running tap water for 1 min. Gill's II haematoxylin (VWR code 1.05175.0500) purchased readymade was used for staining the nucleus. The slides were put in staining jars containing haematoxylin for 90 sec and rinsed in tap water. The slides were then dipped in 1% aqueous eosin (VWR code 34197 2Q) with 1% calcium carbonate (*Sigma C4830*) for 5 min and were again rinsed in running tap water. The slides were then dehydrated by dipping them in serial concentration of IMS and xylene to clear and coverslip was placed after adding 2-3 drops of p-Xylenebispyridinium Bromide (DPX) mountant. Detailed protocols on the timings are given in Fig. 9.

### 2.7.5 TARTRATE RESISTANT ACID PHOSPHATASE (TRAP) STAINING

TRAP staining was done by the standard Napthol AS-BI phosphate post-coupling method. Here the staining was done by adding the substrate Napthol AS - BI phosphate followed by the coupler hexazonium pararosaniline.

#### 2.7.5.1 PREPARATION OF SOLUTIONS

#### ACETATE TARTRATE BUFFER

1.2% acetic acid was prepared by dissolving 6ml of absolute acetic acid (purchased from *Analar Chemicals*) to 494ml of distilled water. 0.2M Acetate buffer was prepared by dissolving sodium acetate trihydrate *(Sigma* S-9513) in 200ml of distilled water. The pH of the resultant solution was adjusted to 5.2 by adding 50ml of 1.2% acetic acid. 4.6 gm of sodium tartrate (*Sigma* S-4797) was added to the 50ml of acetate buffer to form acetate tartrate buffer and covered with foil and warmed to 37°C for 2-4 hrs along

with coplin jars and conical flasks. Dewaxing and hydration of the slides were done according to standard protocol given in Fig. 9 and the slides were placed in the warm buffer for 5 minutes at RT in coplin jars.

## SOLUTION **A**

0.02g of Napthol AS - BI phosphate (*Sigma* N-2250) was dissolved in 1ml of dimethyl formamide (*Fisher Scientific* Catalogue No D/3841/08) in a glass cap and the resultant solution added to the 50ml acetate tartrate buffer. This was the Solution A and the slides were incubated in solution A for 30 min at 37°C.

## SOLUTION **B**

Solutoion B was prepared in a fume hood. 80mg sodium nitrate (*Sigma* S-2252) was added to 2ml distilled water to from 4% sodium nitrate solution. 2ml of pararosaniline (*Sigma* P-3750) was added to the 4% sodium nitrate solution to form hexazonium pararosaniline. All the procedures were carried out in a fume hood. Shortly before the completion of the incubation for solution A, 2.5ml of hexazonium pararosaniline/sodium nitrate solution was added to 50ml of pre-warmed acetate tartrate buffer to form solution B. The slides were incubated in solution B for 15 min at 37°C. The slides were rinsed in tap water and counterstained with Gill's II haematoxylin for 20 sec. The slides were then rinsed again in running tap water and dehydration done according to the protocol given in fig.9 and coverslip was placed after adding 2-3 drops of DPX mountant.

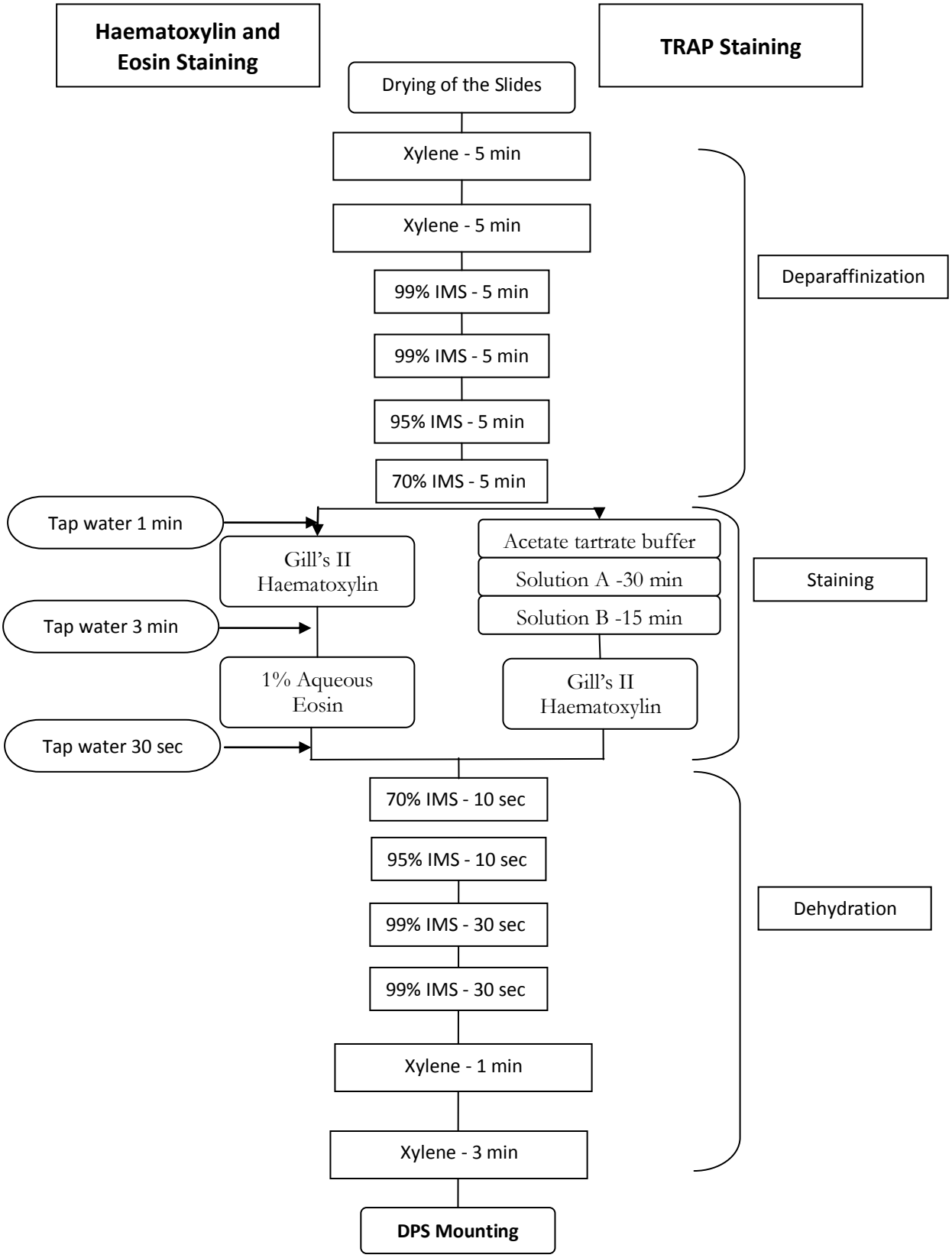


**Figure 9** : Protocol for H&E and TRAP staining

### 2.7.6 BONE HISTOMORPHOMETRY

Lieca LIETZ DMRB microscope connected to a Sony colour video camera

Slides of 5, 7 and 12 weeks male tibia were analysed for this study. Osteomeasure Software, OsteoMetrics Inc, USA was used for the endocortical and trabecular analysis. The camera is adjusted to focus on a field size of 250x250 $\mu m^2$. The slides were analysed using the 10X dry objective. Osteoblast number, osteoclast number, bone perimeter, tissue area and osteoblast and osteoclast surface were measured and analysed.

For Endocortical analysis, 6 fields of size 250x250 $\mu m^2$ were analysed on both the sides at a fixed distance of 250μm from the point of intersection of the growth plate to the cortical bone. The osteoblasts were identified as haematoxylin stained cuboidal cells in groups with eccentrically placed nucleus positioned opposite to the bone forming surface. Osteoclast appears as large multinucleated pink coloured cells in TRAP staining. The endocortical perimeter was measured and the osteoclast and osteoblast surface occupancy on the endocortical region was also traced.

For trabecular analysis, 9 fields of size 250x250 $\mu m^2$ each at a fixed distance of 250 μm from the centre of the growth plate in a 3x3 grid fashion of a total area of 562500$\mu m^2$ were analysed. The trabecular bone area was traced and the osteoblast, osteoclast number and surface occupancy were also measured.

## 2.8 MULTIPHOTON MICROSCOPY

According to the experimental protocol described in chapter 2.4 specimens were obtained from the mice and stored in -80°C. Left tibia samples were used for this analysis and the other specimens were preserved for future analysis.

### 2.8.1 SPECIMEN PREPARATION

#### FREEZING AND CUTTING THE BONE SAMPLE

Tibia samples were frozen and embedded before cutting them in a cryostat. Freezing was done using a hexane/methanol freezing bath. The embedding media used for this purpose was OCT embedding matrix also known as cryo embedding media to ensure optimal cutting temperature (OCT). The hexane/ methanol freezing bath was prepared 20 minutes prior to the start of the freezing the bones. A large glass beaker filled with dry ice was placed inside a polystyrene box filled with dry ice surrounding the beaker on all sides. Methanol was added into the glass beaker slowly till it covered the dry ice filled inside it. A metal container was placed on this dry ice and filled with hexane. Two brass chucks were placed inside this container. Left tibia stripped of soft tissues was placed diagonally inside a plastic mould of 19mm size and covered with OCT media then placed on a brass chuck inside the metal container until the OCT froze. The position of the left tibia placed inside the plastic mould is shown in fig. 10.

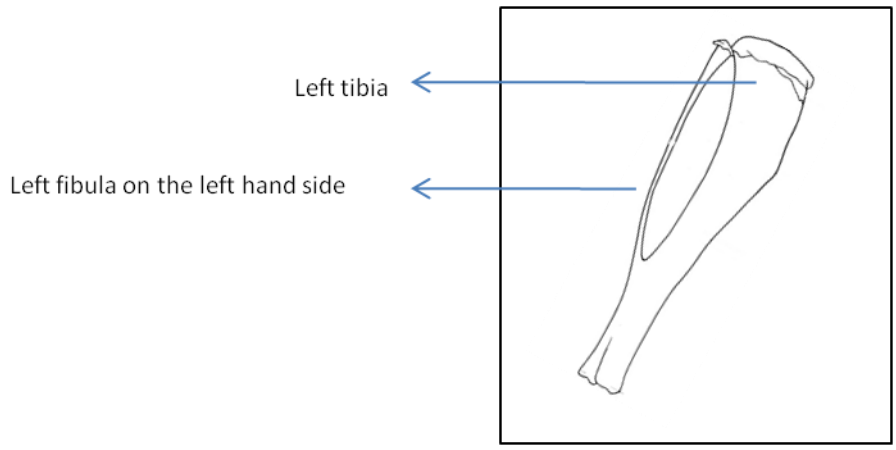


**Figure 10**: Orientation of Tibia in the plastic mould before freezing in the OCT.

Frozen specimens were then cut using a Cryostat 5030, Bright Instrument Company, UK. Frozen sections were initially trimmed to the bone surface, then approximately around 900 micron depth was cut away (this varies with each bone) till the growth plate was exposed and the bone marrow was visible for the whole length of the tibia.

### 2.8.2 MULTIPHOTON MICROSCOPY IMAGING AND ANALYSIS

Zeiss LSM 510 Meta Inverted Microscope equipped with coherent chameleon laser for Multiphoton Imaging

Phosphate-Buffered Saline (PBS) 7.4 (1X) liquid (Catalogue No. 10010-023) from Invitrogen was used to remove the tibial samples from the OCT prior to multiphoton scanning. The flat cut surface of the tibia was placed in a small petri dish and loaded onto the microscope. Initial visualization of the specimen was done using the X20 dry piece objective lens and the pilot image was scanned using an emission band pass filter of 435-485nm with a 128x128 pixel size for quicker scanning. A reference point was chosen in the tibial metaphysis at a distance of appropriately 450µm from the growth plate and a ROI was chosen and a tiled 'Z' stack in a 3 X 4 grid fashion with each tile at 450x450µmm$^2$ was scanned at a resolution of 512x512 pixels size and a depth of 75µm within the bone tissue. A clear description of the position of the ROI from the growth plate is shown in fig.11 in comparison with the actual scanned image. The Zeiss LSM 510 Meta is equipped with a coherent chameleon laser set at a 900nm wavelength. An emission band pass filter of 500-550nm was used to visualise GFP expressing PC3 cells while the normal bone tissue using second harmonic generation was imaged using an emission band pass filter of 435-485nm wavelength. The scanned images were reconstructed and analysed using the software Volocity® ver 5.2.0 ©2007, Improvision Ltd.

The reference range of the PC3-GFP-Tib3 cell volume in a multiphoton microscopy was determined by scanning *in vitro* adherent PC3-GFP-Tib3 cell culture using the same parameters which was used for scanning the tibia samples of the test animals. Multiphoton microscopy image of the *in vitro* cell culture of PC3-GFP-Tib cell is shown in fig. 20. The colour intensity was set at 500 for visualising GFP and the volume of object within the colour range were analysed and computed. The lowest volume object with colour intensity of 500 and above was observed to have a size of 1001.9cu. µm. The background intensity for analysis was set using the colour intensity values obtained from scanning the control sample.

Based on these parameters the analysis was done on the test images and the objects visualised with a colour intensity of 500 with a volume less than a 1000 cu.μm were excluded from the analysis as the minimum volume of PC3-GFP-Tib3 cell observed from the *in vitro* culture was above 1000 cu.μm. The data's were analysed and computed.

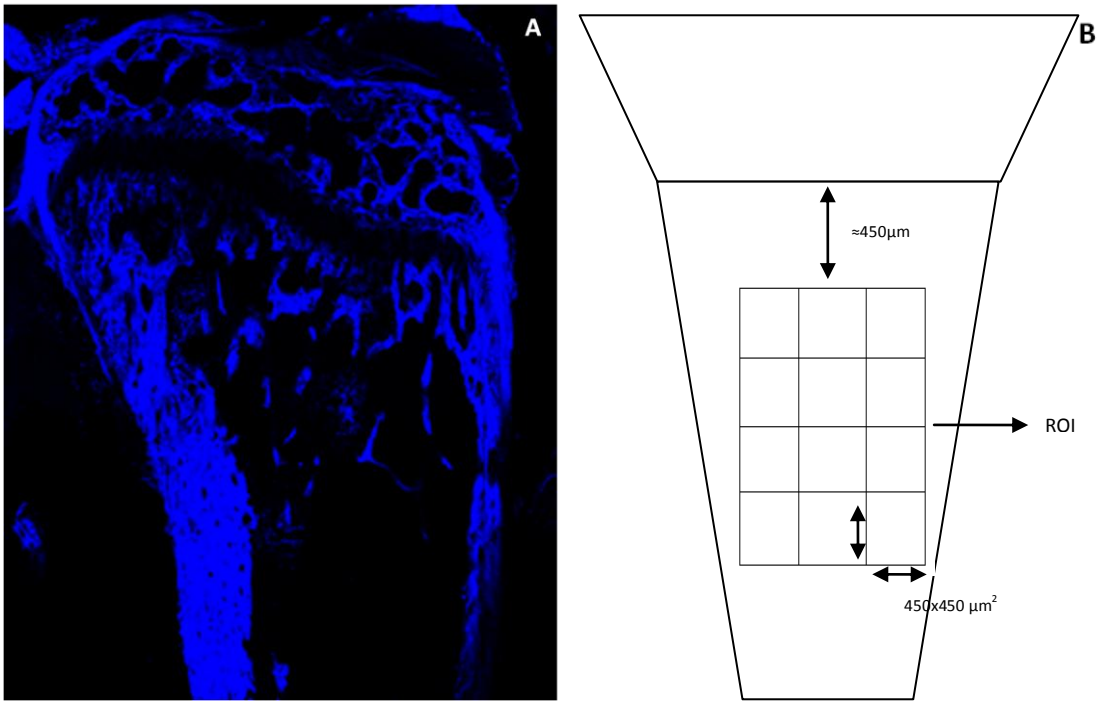


**Figure 11:** Multiphoton Microscopy image of the tibia

A. 2D Pilot image of the whole tibia scanned using the emission bandpass filter of 435-485nm wavelength.
B. Schematic representation of the ROI, 3x4 grid of size 450x450 µm² each.

## 2.9 STATISTICAL ANALYSIS

Comparison within groups was done using one-way ANOVA with post test - Bonferroni compare all pairs of columns. Statistical significant in the age by sex interaction was calculated using a two-way ANOVA. Comparison in the differences among sexes was done using a non-parametric students 'T' test. GraphPad Prism software ver 5.01 was used for statistical analysis and Microsoft Excel 2007 for plotting graphs.

# CHAPTER 3 RESULTS

## 3.1 AGE AND SEX RELATED CHANGES IN TRABECULAR PARAMETERS IN TIBIAE AND VERTEBRAE OF NOD/SCID MICE

In this initial study of age and sex related changes in NOD/SCID mice were looked at in tibiae and $L_1$ lumbar vertebrae.

### *Trabecular bone volume, trabecular thickness and bone mineral density increased with increase in age in tibia and vertebra in both male and female NOD/SCID mice*

Figure 12(A) shows significant age related change in trabecular BV/TV in the tibiae between 5 and 14 weeks in male NOD/SCID mice ($P<0.05$), whereas no statistically significant growth was seen between the rest of the group. However a pattern of increase in trabecular BV/TV was observed from 5 to 14 weeks. Similarly in the female mice, however a growth pattern existed from 5 to 14 weeks like their male partners statistically significant growth was observed early at 12 weeks (Fig 12A). A comparative analysis between male and female done using Students 'T' Test showed significant difference in trabecular volume was observed only among animals of 5 weeks age (Fig. 12A). No age by sex interaction was observed calculated by two-ANOVA in the trabecular BV/TV of tibia (Table 2).

No significant change in Tb.N of tibia was observed throughout the study group (5-14 weeks) in both the sexes (Fig. 13C). A steady increase in the Tb.Th was observed in both the sexes (Fig. 13A & 15). A significant increase in the Tb.Th was observed between 5 and 6 weeks and attains a steadier plateau phase thereafter in males whereas in females a similar pattern with significant growth in the trabecular thickness was observed between 5 and 7 weeks. Trabecular thickness doesn't seem to change overall between both the sexes from 6-14 weeks. However said so, female mice seem to have an increased Tb.Th compared males though not statistically significant. This reflects the reduction in Tb.pf (trabecular connectivity) and SMI (rods to plate like structure of the trabeculae) in females' in spite of a lesser Tb.N compared to males. There is an overall declination in the Tb.pf observed in both the sexes, with no significant changes observed between males and females during 5 and 6 weeks after which they were much lower in females. Significant increase in the BMD was observed in both the sexes from 5 to 14 weeks with $P<0.0001$ in both sexes. SMI increased in males and decreased in females from 5 to 14 weeks (2.61% increase in males; 23.71% decrease in females) (Table 1).

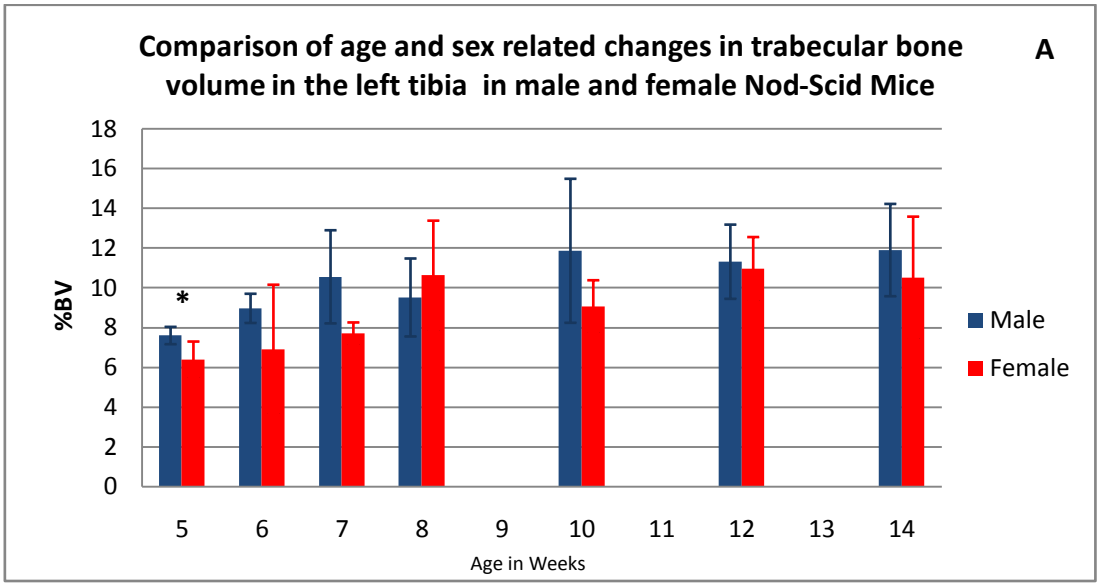


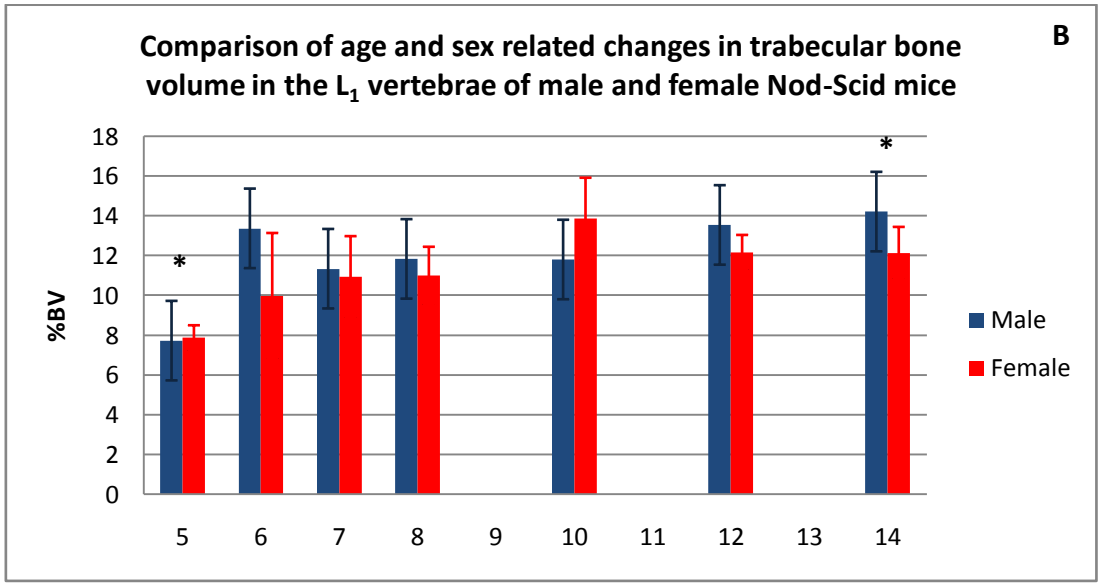


**Figure 12**: Age and Sex related changes in Trabecular bone volume

**A.** Mean ± SD of %BV bone volume in left tibia.

**B.** Mean ± SD of %BV in $L_1$ vertebrae.

***** Significant difference between sexes.

Similar pattern were observed in the $L_1$ lumbar vertebrae, however increase in BV/TV was higher in both sexes compared to tibia especially in females. Increased trabecular growth was observed between 5 and 10 weeks in females after which it declined and plateaued whereas in males it was observed till 12 weeks. Tb.Th increased in both the sexes (Fig. 13B), like in the tibia. No significant difference was observed between both the sexes at any time point or age by sex interaction was observed. Significant increase in Tb.N observed in males from 5 to 14 weeks with an overall increase of 35.8% was observed (Figs. 13C, Table 1). No significance was observed among females however the pattern shows an increase from 5 to 10 weeks and gradually decline thereafter. Tb.pf significantly decreased in both the sexes with increase in age (Fig. 13F). Unlike tibia, the SMI decreased markedly in males ($P=0.0006$) describing a more rod-like structures in the vertebrae (Fig 13H), compared to tibia was composed of more plate-like trabeculae. In females no significant change was seen. The pattern of increase in the BMD was similar what was observed in the tibia with a steady increase from 5 to 8 weeks after which it plateaued till 10 weeks and rise again. Statistically significant increase in BMD was observed in both the sexes. Age by sex interaction was observed only between trabecular BV/TV and BMD in the vertebrae (Fig. 13J).

## 3.2 AGE AND SEX RELATED CHANGES IN THE CORTICAL PARAMETERS IN TIBIA

### *Cortical Volume increases in females from 5 to 14 weeks*

Cortical analysis was done in tibia using μCT to assess the change in the Ct.V and the BMD of cortex with increase in age within a time frame of 5 to 14 weeks. A significant increase in the Ct.V was observed with an overall gain of 26.08% in the cortical bone in females from 5 to 14 weeks ($P<0.0001$). In males no significant change was observed throughout the study group (Fig. 14B). However significant increase in BMD was observed in both the sexes with more in females to males in 5, 6, 7 and 14 weeks. Significant age by sex interaction was observed in cortical BMD ($P<0.05$) (Fig. 14A).

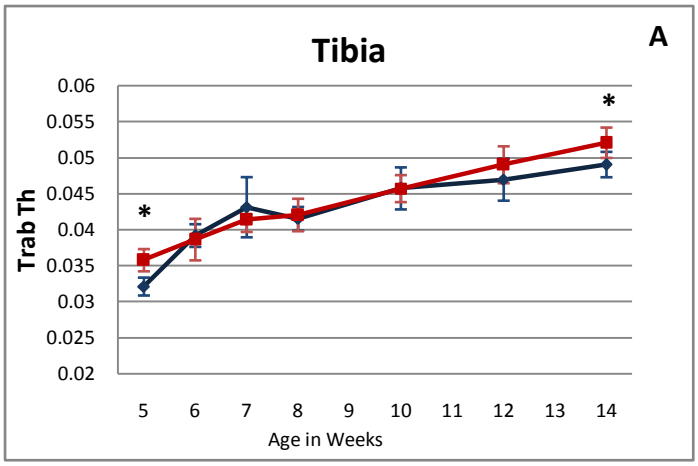
A
Tibia
Trab Th
0.06
0.055
0.05
0.045
0.04
0.035
0.03
0.025
0.02
5 6 7 8 9 10 11 12 13 14
Age in Weeks
*
*

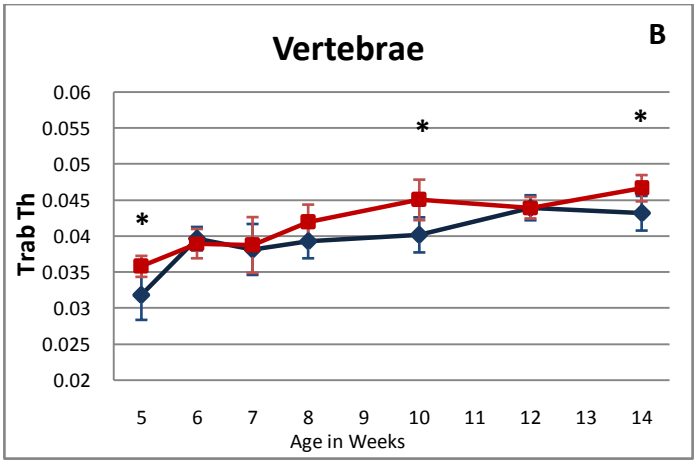
B
Vertebrae
Trab Th
0.06
0.055
0.05
0.045
0.04
0.035
0.03
0.025
0.02
5 6 7 8 9 10 11 12 13 14
Age in Weeks
*
*
*

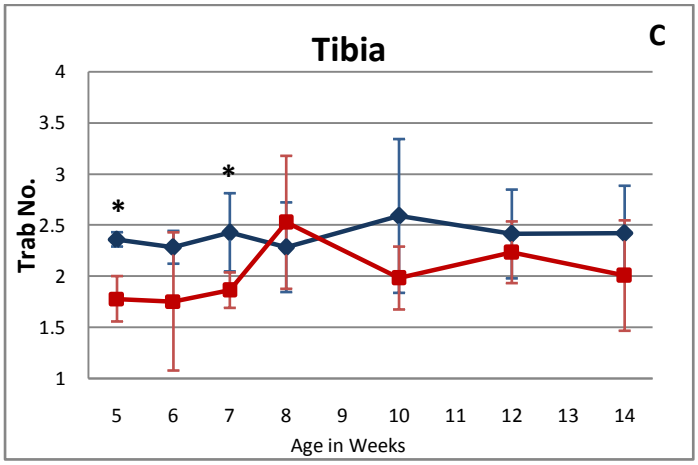
C
Tibia
Trab No.
4
3.5
3
2.5
2
1.5
1
5 6 7 8 9 10 11 12 13 14
Age in Weeks
*
*

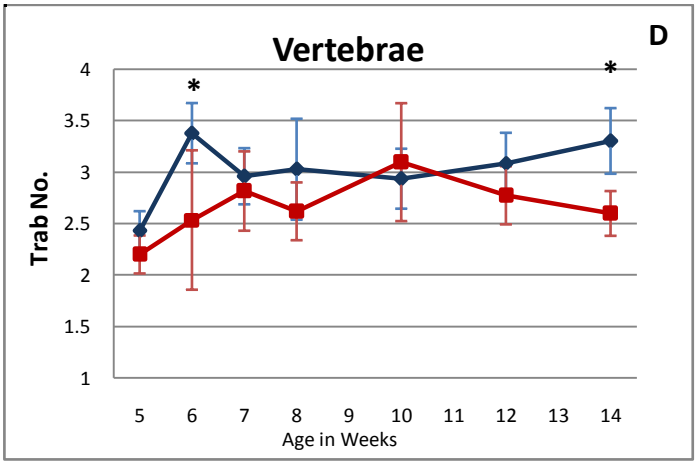
D
Vertebrae
Trab No.
4
3.5
3
2.5
2
1.5
1
5 6 7 8 9 10 11 12 13 14
Age in Weeks
*
*

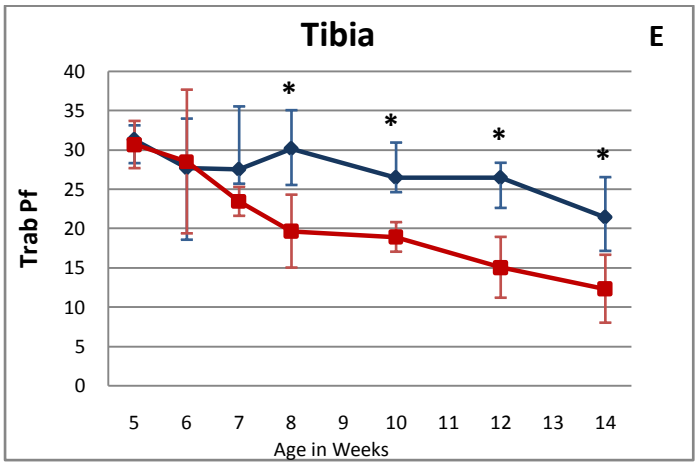
E
Tibia
Trab Pf
40
35
30
25
20
15
10
5
0
5 6 7 8 9 10 11 12 13 14
Age in Weeks
*
*
*
*

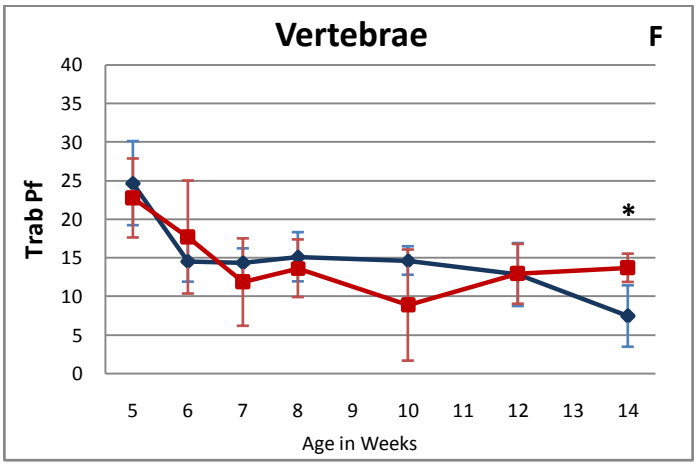
F
Vertebrae
Trab Pf
40
35
30
25
20
15
10
5
0
5 6 7 8 9 10 11 12 13 14
Age in Weeks
*

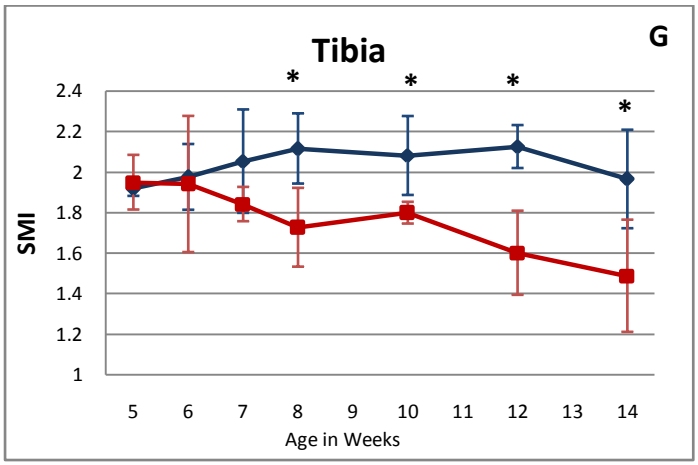
G
Tibia
SMI
2.4
2.2
2
1.8
1.6
1.4
1.2
1
5 6 7 8 9 10 11 12 13 14
Age in Weeks
*
*
*
*

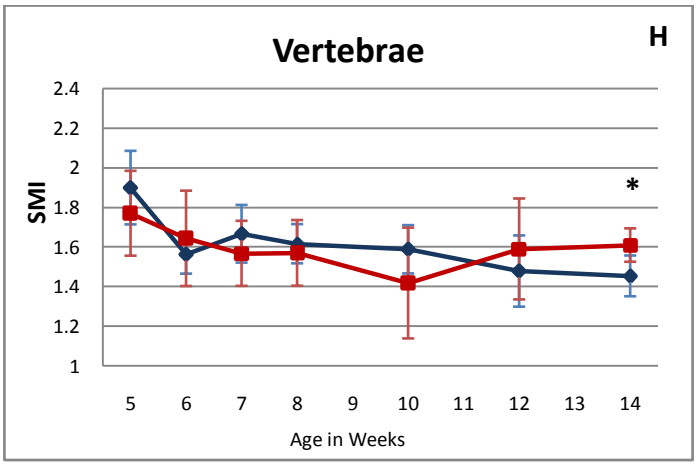
H
Vertebrae
SMI
2.4
2.2
2
1.8
1.6
1.4
1.2
1
5 6 7 8 9 10 11 12 13 14
Age in Weeks
*

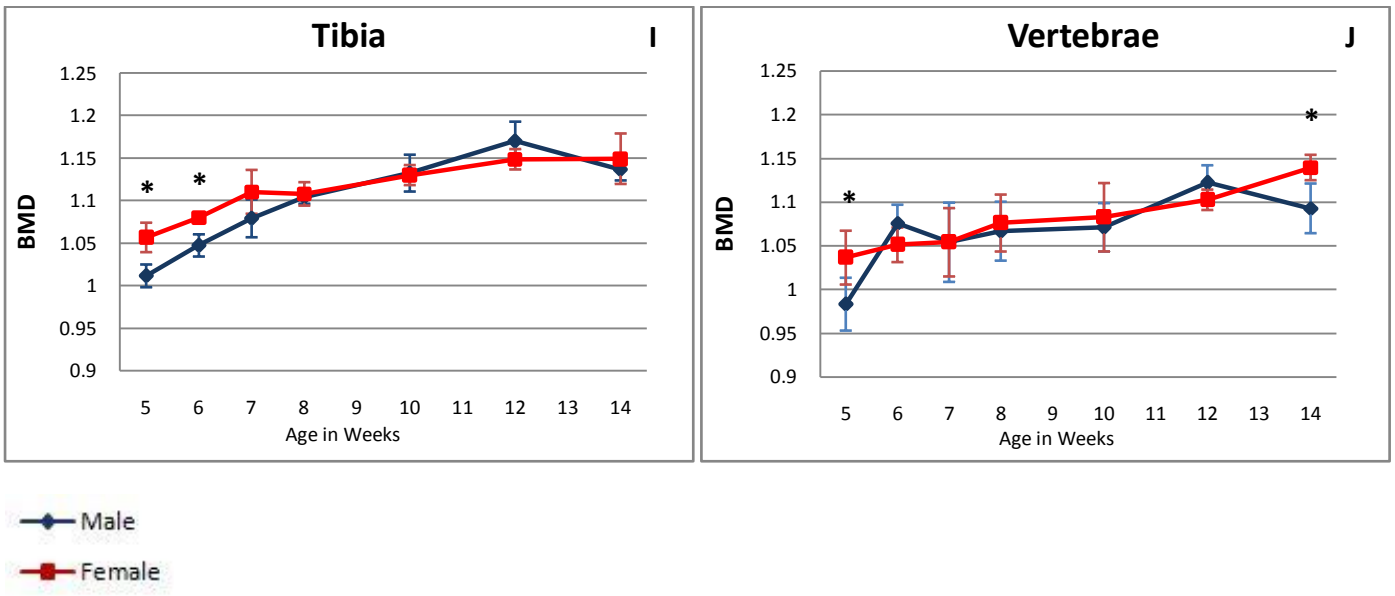


**Figure 13**: Age and sex related changes in trabecular parameters in left tibia and $L_1$ lumbar vertebrae by μCT (Mean ± SD) in male and female NOD/SCID mice from 5 to 14 weeks.

* Significant difference between sexes was compared using non-parametric two tailed Students 'T'test.

## CORTICAL ANALYSIS IN LEFT TIBIA

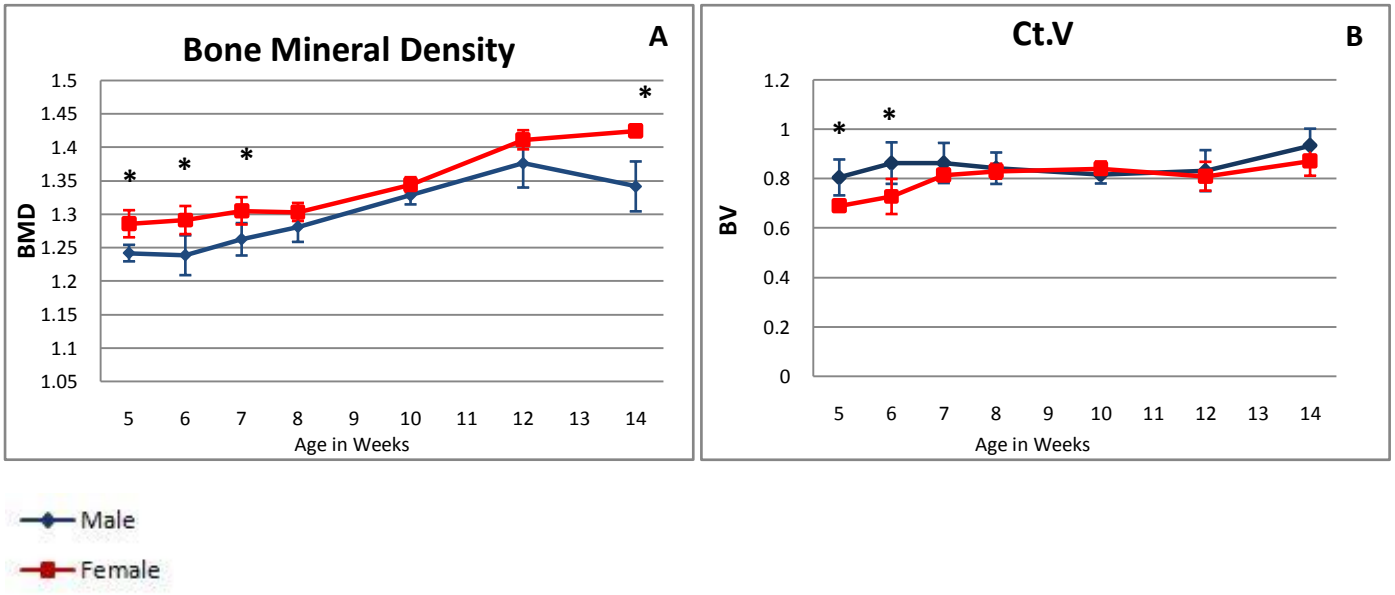


**Figure 14:** Changes in the cortical BMD and cortical volume of left tibia in male and female NOD/SCID mice.
* Significant difference between sexes was compared using non-parametric two tailed Students 'T'test.

**Table 1: Comparative study of trabecular parameters in male and female NOD/SCID mice aged 5-14 weeks, assessed by µCT**

| | Males | | Females | |
|---|---|---|---|---|
| | *Mean ±SE at 5 weeks* | *% change from 5 to 14 weeks ** | *Mean ±SE at 5 weeks* | *% change from 5 to 14 weeks* |
| **Left Tibia** | | | | |
| BV/TV (%) | 7.58 ± 0.19 | 55.67% | 6.37 ± 0.4 | 64.54% |
| Trab Th (µm) | 0.03 ± 0.0005 | 63.33% | 0.03 ± 0.0006 | 48.57% |
| Trab Pf. | 31.3 ± 0.8 | -31.43% | 30.67 ± 1.34 | -59.79% |
| Trab No. | 2.36 ± 0.03 | 2.54% | 1.77 ± 0.099 | 12.99% |
| SMI | 1.91 ± 0.01 | 2.61% | 1.94 ± 0.06 | -23.71% |
| BMD | 1.01 ± 0.005 | 12.47% | 1.05 ± 0.007 | 8.8% |
| Cortical Volume (EcV) | 0.80 ± 0.03 | 16.2% | 0.69 ± 0.0102 | 26.08% |
| **L1 Lumbar Vertebrae** | | | | |
| BV/TV (%) | 7.73 ± 0.37 | 83.95% | 7.87 ± 0.28 | 54.25% |
| Trab Th (µm) | 0.03 ± 0.0015 | 38.71% | 0.03 ± 0.0006 | 33.33% |
| Trab Pf. | 24.65 ± 2.43 | -69.77% | 22.73 ± 2.28 | -39.77% |
| Trab No. | 2.43 ± 0.08 | 35.80% | 2.20 ± 0.08 | 17.72% |
| SMI | 1.89 ± 0.08 | -23.64% | 1.76 ± 0.09 | -9.09% |
| BMD | 0.098 ± 0.01 | 11.08% | 1.04 ± 0.01 | 9.70% |

* Percentage change of mean from 5 to 14 weeks was calculated.

**Table 2:** Comparison of age related changes between sexes and age by sex interaction

| | P Value | |
|---|---|---|
| | *Male Vs Female at 5 weeks of age* ** | *Age by sex interaction from 5 to 14 weeks*++ |
| **Left Tibia** | | |
| BV/TV (%) | 0.0377 | *ns* |
| Trab Th (µm) | 0.0036 | *ns* |
| Trab Pf. | *ns* | 0.035 |
| Trab No. | 0.0029 | *ns* |
| SMI | *ns* | 0.0136 |
| BMD | 0.0020 | 0.0012 |
| Cortical Volume (EcV) | 0.0212 | |
| **L1 Lumbar Vertebrae** | | |
| BV/TV (%) | *ns* | 0.0117 |
| Trab Th (µm) | *ns* | *ns* |
| Trab Pf. | *ns* | *ns* |
| Trab No. | *ns* | *ns* |
| SMI | *ns* | *ns* |
| BMD | 0.0275 | 0.0265 |

** Unpaired T test with 2 tailed distribution.
++ Age by sex interaction in two-way ANOVA using Bonferroni post test.

**MALE**

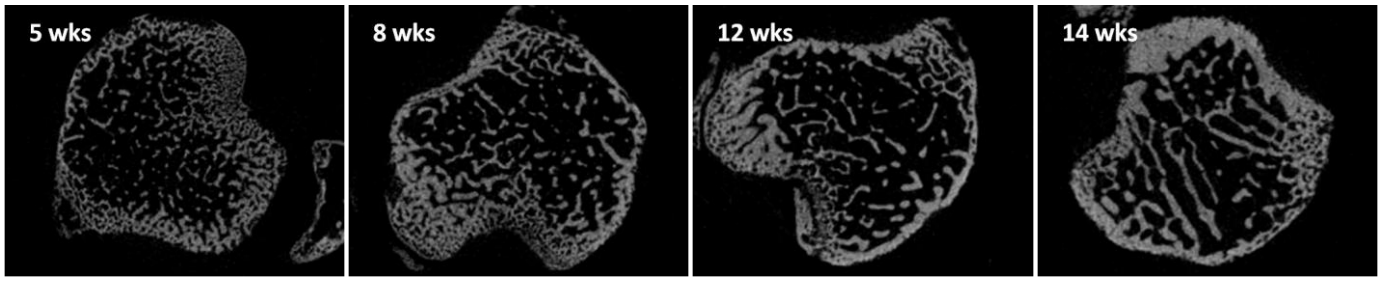


**FEMALE**

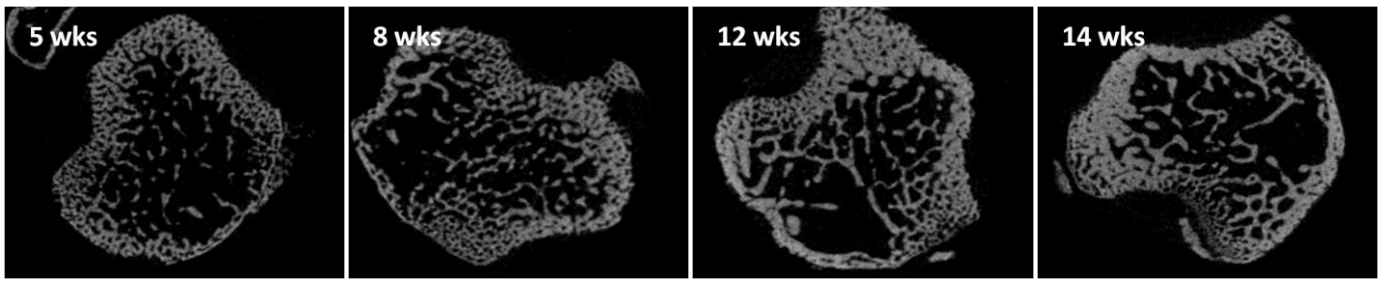


**Figure 15:** Age related changes in the trabecular architecture in male and female NOD/SCID mice by μCT.

The above images illustrate the trabecular architecture of the tibial metaphysis at a fixed distance (50μm) from the reference point. The reference point is the break in the distal aspect of the growth plate. A gradual increase in the trabecular BV and cortical BV is observed with increase in the age of the mice in both male and female.

Thickening of the trabeculae with widening of the distance between individual trabecula can also be noted.

## 3.3 BONE FORMATION AND RESORPTION MARKER REDUCE WITH INCREASE INAGE

### *Pro-collagen 1 N-terminal propeptide concentration falls with increase in age in both male and female NOD/SCID mice*

Cellular activity during bone turn-over was determined by assessing the levels of bone formation and bone resorption markers. Inverse co-relation was observed between age and PINP concentration in NOD/SCID mice with the peak value seen in the age group of 5 weeks (Fig. 16). Male mice at 5 weeks had a significantly higher concentration of PINP compared to females of the same age. There is a rapid fall in the PINP concentration observed between 5 and 6 weeks of age in male group after which is reduction in PINP level was steadier. Unlike males, gradual reduction in PINP levels was observed in female mice from 5 to 14 weeks. No significant difference was observed in the PINP concentration in both male and female mice older than 7 weeks ($P > 0.05$). Significant reduction in PINP levels were observed between 5 and 7 weeks mice in both female and male groups ($P=0.009$ in males and $P=0.0005$ in females)(Table 3). Significant age by sex interaction in the PINP levels were observed (Table 3)

### *C-Telopeptide Type I collagen concentration falls with increase in age in both male and female Nod-Scid mice*

Similar to PINP, reduction in the levels of CTX was observed in both the sexes with increase in age from 5 to 14 weeks (Fig. 17). Rapid fall in the level of CTX was observed in males from 5 to 8 weeks after which the reduction in CTX level attained a steadier pace. Significant difference was observed between 5 and 6 weeks ($P<0.05$) whereas in females significance was observed in 7 weeks. The fall in CTX levels in females were gradual compared to males. No significant difference was observed between the sexes at any time points. Comparison was done using non-parametric two-tailed Students 'T' test. No age by sex interaction was observed in the CTX levels (Table 3).

**Table 3:** Age and sex related difference in bone turn-over markers

| | Male | | Female | | *Male Vs Female at 5 weeks of age* ** | *Age and sex interaction*++ |
|---|---|---|---|---|---|---|
| | *Comparison of 5 weeks with the group** | *Mean ± SE* | *Comparison of 5 weeks with the group** | *Mean ± SE* | | |
| PINP | <0.0001 | 95.31±16.15 | <0.0001 | 30.01±4.51 | 0.0133 | <0.0001 |
| RatLaps CTX | <0.0001 | 55.07±5.27 | 0.0002 | 48.15±2.8 | *ns* | *ns* |

* Comparison of 5 weeks animal was done using one-way ANOVA with Bonferroni post test comparison of 5 weeks with the rest of the group.
** Comparison between sexes was done using non-parametric Students 'T' test.
++Age and sex interaction compared using two-way ANOVA with Bonferroni post test.

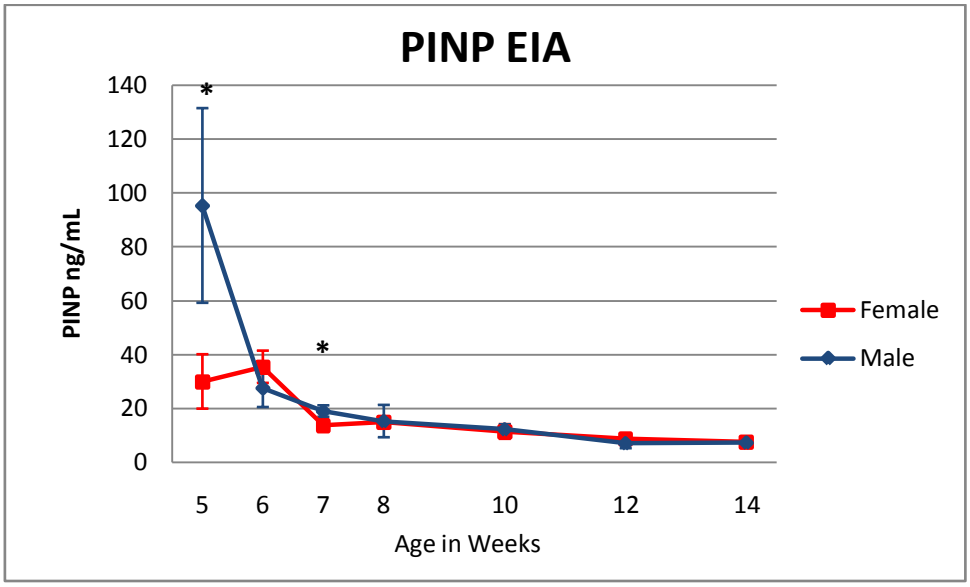


**Figure 16:** Changes in P1NP levels in ng/mL in both female and male NOD/SCID mice from 5 to 14 weeks

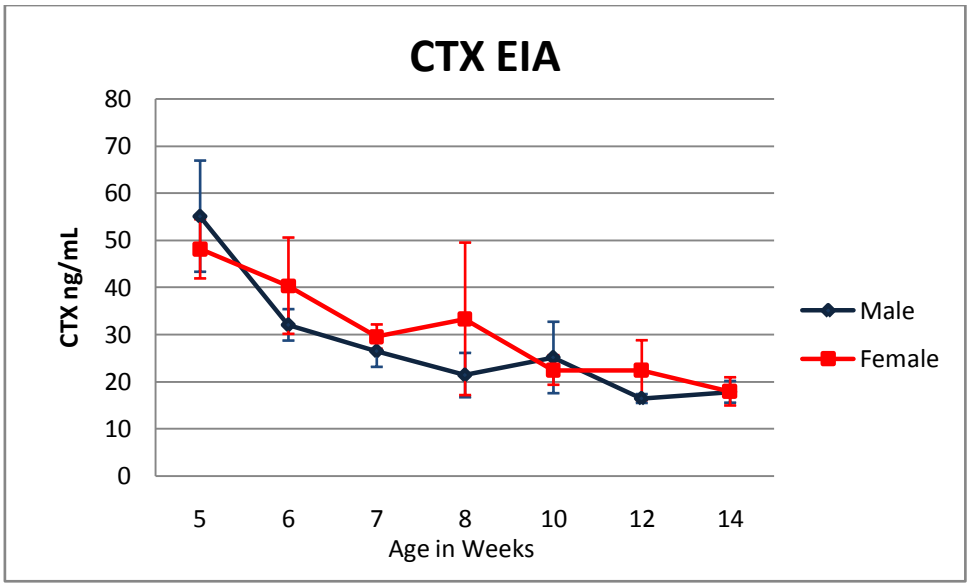


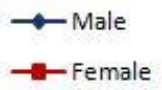


**Figure 17**: Comparison of CTX levels in ng/mL in male and female NOD/SCID mice from 5 to 14 weeks.
* Significant difference between sexes was compared using non-parametric two tailed Students 'T'test.

## 3.4 AGE RELATED CHANGES IN CELLULAR COMPOSITION OF TIBIA

***Osteoblast number and percentage surface occupancy decrease in both the trabecular and endocortical region with increase in age from 5 to 12 weeks in male NOD/SCID mice***

Static histomorphometry examinations were done on left tibia slides stained with TRAP. Only 5, 7 and 12 weeks of age male tibiae were analysed. Both endocortical and trabecular parameters were documented and analysed. Gradual reduction in the osteoblast number was observed from 5 to 7 weeks but never reached significant levels in both the endocortical and trabecular region. However significant reduction in the osteoblast number was observed from 7 to 12 weeks both in the endocortical and trabecular region. In the endocortical region, significant reduction from 7 to 12 with a $P<0.05$ was observed with a 3 fold decrease in the osteoblast number per mm of the endocortical bone perimeter from 5 to 12 weeks. Similar pattern were observed in the trabecular region analysis with a 3-4 fold decrease from 5 to 12 weeks (Fig 18 A, E). Interestingly in the endocortical analysis, there exists a site dependant variation in the osteoblast population in the tibia with increased osteoblasts residing in the endocortical region of the postero-lateral aspect of the tibia and near the growth plate of mice between 5 and 12 weeks of age (Appendix III).

Percentage surface occupancy of the osteoblast was calculated for both the endocortical and the trabecular region using the osteoblast perimeter (Ob.Pm) and the bone perimeter (B.Pm in trabecular and Ec.Pm in endocortical region).

Statistical significance in the differences among the age groups was calculated using non-parametric students 'T' test. A small increase in the surface occupancy was observed between 5 to 7 weeks in the trabecular region followed by a more dramatic fall from 7 to 12 weeks age ($P<0.05$). In the endocortical region there is a gradual fall observed from 5 to 12 weeks whereas significant difference was observed only between 7 to 12 weeks ($P<0.05$) (Fig 18 E, F).

***No significant change observed in osteoclast number and surface occupancy in both the trabecular and endocortical region with increase in age from 5 to 12 weeks in male Nod-Scid mice***

No significant change observed in both the osteoclast number and the percentage surface occupancy was observed. The reason for this might be the very high SD observed among the age groups of mice. However a pattern of decline in the osteoclast number and surface occupancy was observed with increase in the age. (Fig. 18 B, D, F, H,)

The complete result of osteoclast and osteoblast parameters as assessed by histomorphometry is furnished in Appendix III & IV.

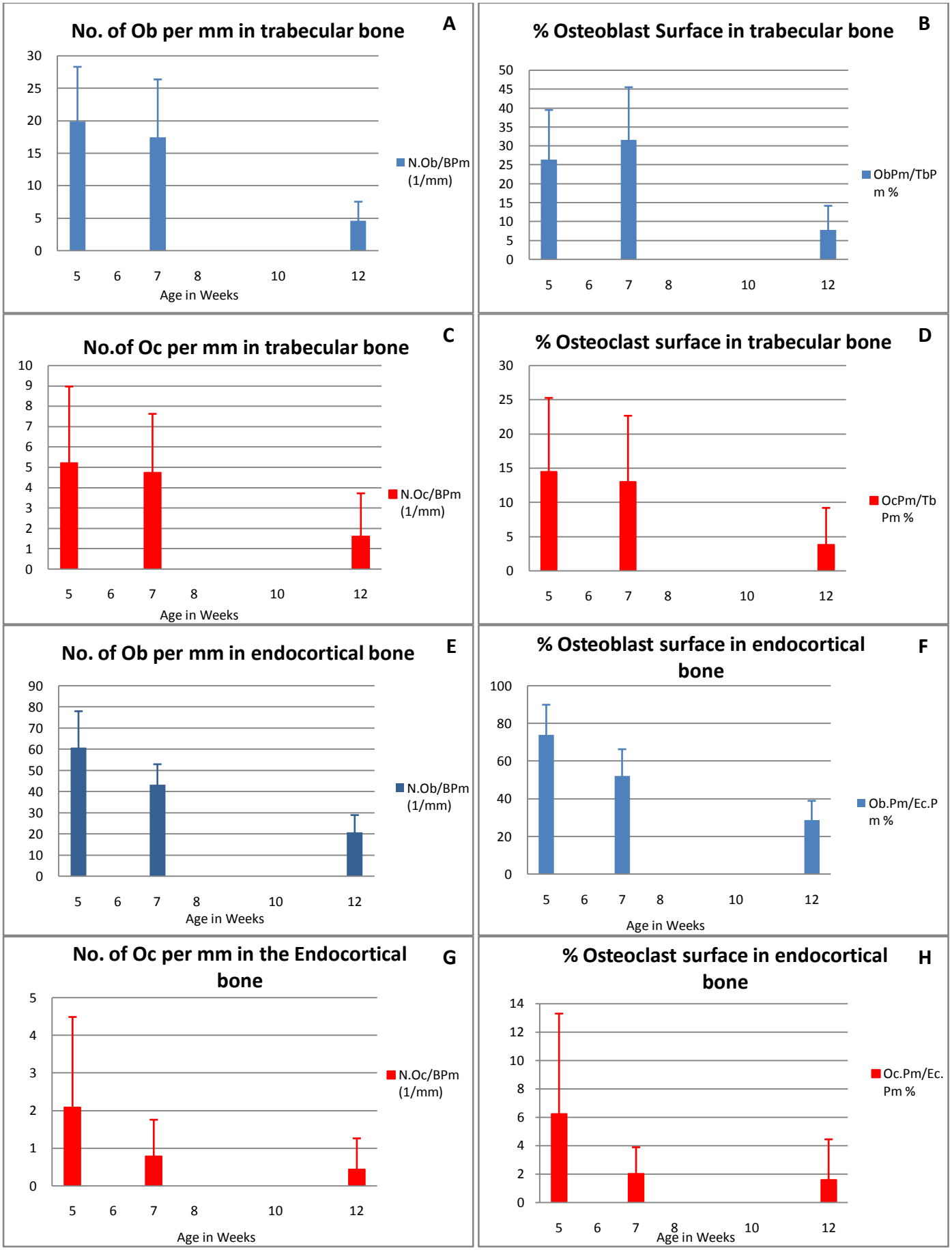


Figure 18: Age related changes in the osteoblast and osteoclast parameters in male NOD/SCID mice as assessed by bone histomorphometry.

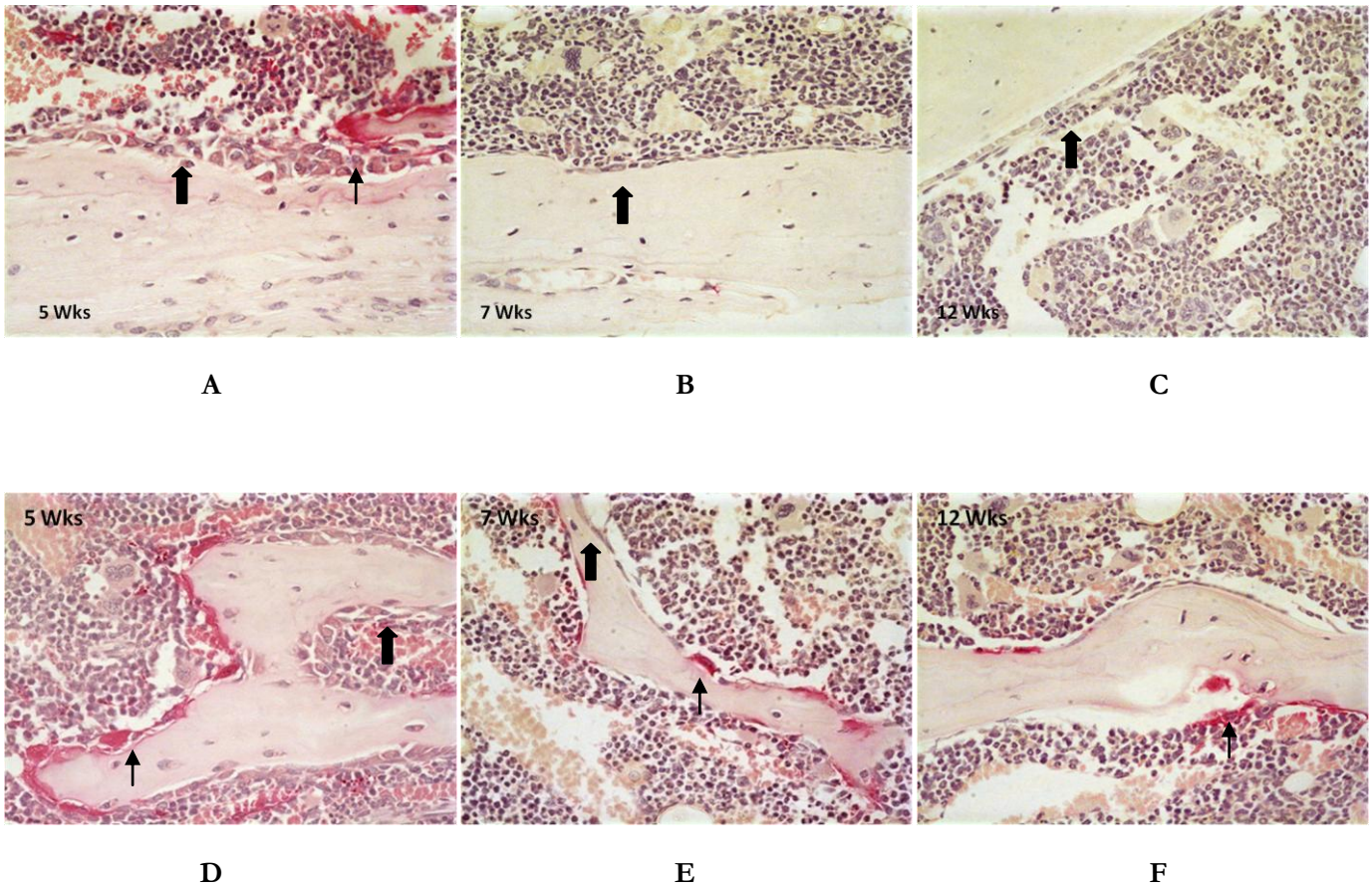


**Figure 19:** Age related changes in the cellular composition in male tibia assessed by histomorphometry.

i. A, B and C show the distribution on osteoclast and osteoblast in the endocortical surface of left tibia in NOD/SCID mice age 5, 7 and 12 weeks respectively.
ii. D, E and F show the distribution on osteoclast and osteoblast in the trabecular region of left tibia in NOD/SDCID mice age 5, 7 and 12 weeks respectively.
iii. Osteoclasts are marked in broad arrows and osteoblast in thin arrows.

## 3.5 VISUALIZATION OF PC3-GFP-TIB3 CELLS IN THE TIBIAL METAPHYSIS USING MULTIPHOTON MICROSCOPY

GFP labelled PC3 cells were injected in male NOD/SCID mice aged 5 weeks and were periodically sacrificed after 18hrs, 48hrs and 1 week respectively. Each group consisted of 5 animals, 4 injected with tumour cell and 1 served as control. The left tibiae were scanned by multiphoton microscope. Fluorescent green cells were visualised in the tibial metaphysis at all the three time points (18hrs, 48hrs and 1 week)(Fig 22). There was a reduction in the average number of GFP positive cells to the bone from 18hrs to 48hrs and then to 1 week (Table 4)(Fig 23B). However, the difference between them was not significant and was due to the high variability observed within the samples of the same age group. In addition to increase in the cell number from 18 to 48hrs post inoculation, there was also an increase in the average volume per cell observed from 18 to 48hrs however, not reached significance (Fig 23A). There was a reduction in both the cell number and cell volume of the GFP positive cells after 1 week. The background was matched with age related negative controls sacrificed at the same time as the test animal, to rule out auto-fluorescence and background noise. Fig 20 illustrates the normal *in vitro* GFP positive PC3 cells used for determining the average volume range of a single PC3-GFP cell. Analysis and determination of cell count and cell volume was done using the Volocity software. An age matched negative control was used for determining the normal background and any auto-florescence emitted by the normal cellular component of the bone (Fig 21). No significant auto-florescence interfering with the analysis was observed.

**Table 4:** Average No. of the GFP positive cell visualised using multiphoton microscopy at 3 different time points in 5 weeks male NOD/SCID mice

| | No. of cells Mean ± SD | Vol./cell Mean ± SD (cu.μm) |
|---|---|---|
| 18hrs *(n=3)* | 17 ± 22.71 | 3649.56 ± 1766.43 |
| 48hrs *(n=4)* | 15 ± 20.21 | 6776.75 ± 9485.69 |
| 1 week *(n=3)* | 5 ± 2.64 | 3085.88 ± 1327.69 |

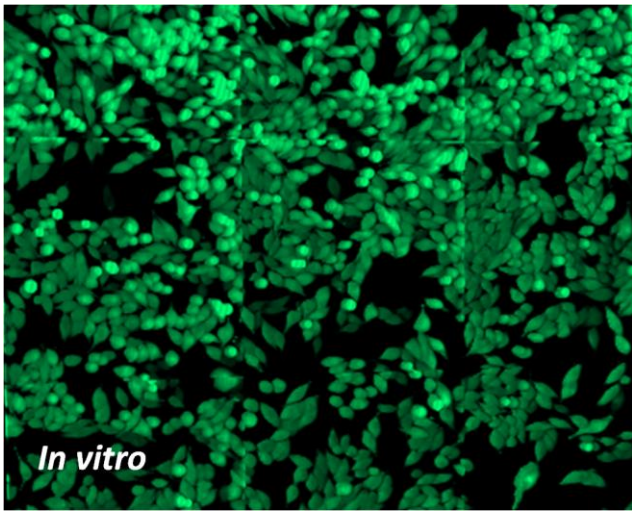


*In vitro* PC3-GFP-Tib3 cell culture visualised under multiphoton microscopy using a 20x dry objective.

**Figure 20:** Multiphoton microscopy picture of PC3-GFP-Tib3 cell in *in vitro* culture

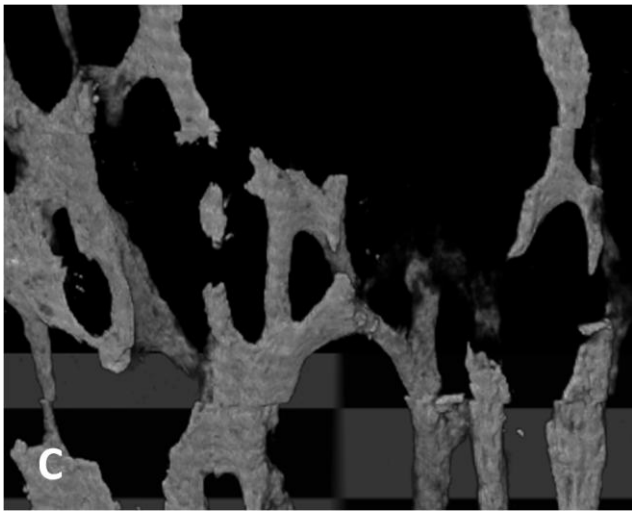


Control sample - Multiphoton microscopy image of tibial metaphysis from normal 5 weeks NOD/SCID male mice sacrificed after 18hrs.
Image shows normal trabecular architecture in the tibial metaphysis as seen after reconstruction of the images using Volocity®

**Figure 21:** 3D image of tibial metaphysis of the control mice

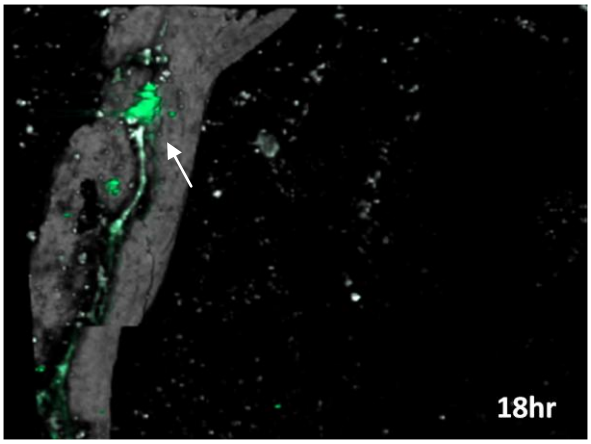


3D 'Z' stack image of tibial metaphysis from 5 weeks NOD/SCID sacrificed after 18hrs of GFP expressing tumour cell injection showing small groups of green fluorescent cells adjacent to the bone

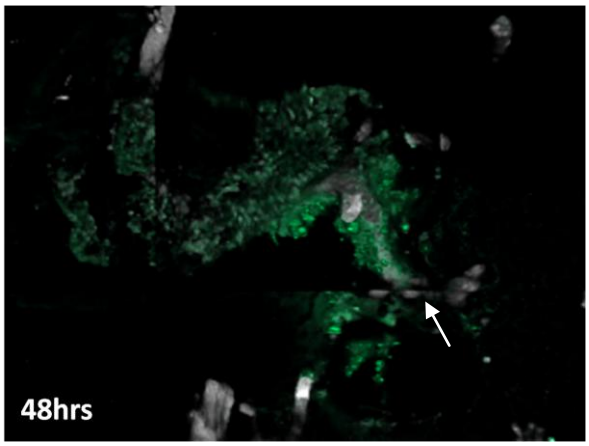


3D 'Z' stack image of tibial metaphysis from 5 weeks NOD/SCID mice sacrificed after 48hrs of tumour cell injection showing a large cluster of green fluorescent cells in the adjacent to the trabecular bone.

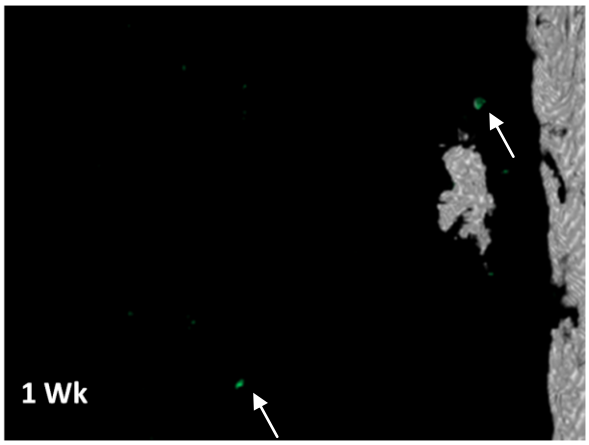


Individual green fluorescent cells (shown by arrows) seen in the tibial metaphysis after 1 week of GFP expressing tumour cell injection.

**Figure 22:** 3D 'Z' stack image of left tibia in NOD/SCID mice sacrificed after 18, 48hrs and 1 week respectively showing clusters and single GFP positive cells in the tibial metaphysis.

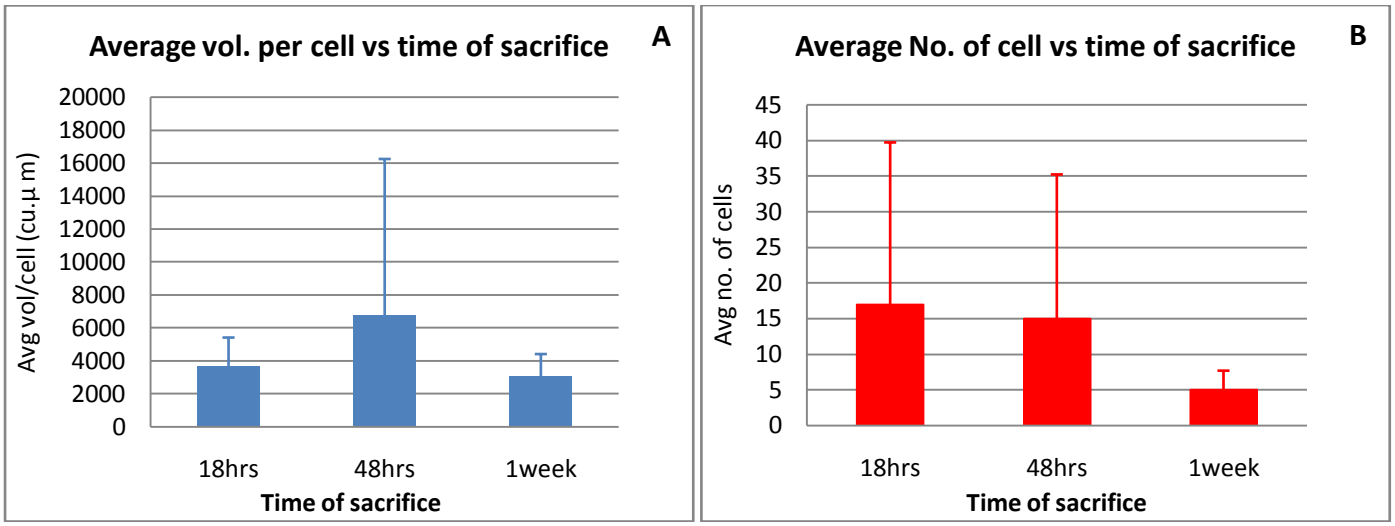


**Figure 23:** Characterising GFP positive cell count and volume in 5 weeks NOD/SCID mice.

# CHAPTER 4 DISCUSSION AND CONCLUSION

Characterizing the age and sex related change in the bone structure and turnover in pre-clinical murine models is important to understand the normal skeletal biology and the interaction with bone. With an increase in the use of murine models as pre-clinical animal models of prostate cancer research, knowledge of the murine bone biology will contribute researchers to have a better understanding of the disease condition, interaction of the xenograft cell line with the murine biological environment and help in the development of novel targets and newer therapeutic approach. Many studies have established the age related changes in the bone turnover in different rodent models and the relationship between bone turnover and tumour take rate. However, no study has so far looked into the age and sex related changes in NOD/SCID mice which are being increasingly used in cancer research. The principal aim of our study was to determine the bone turnover rates in young NOD/SCID mice and scrutinize the usefulness of this strain in prostate cancer bone metastasis research.

The present study suggests an increase in cortical and trabecular bone density in the proximal tibial metaphysis in young male and female NOD/SCID mice with increase in age. In male NOD/SCID mice, a steady increase in the trabecular bone volume was observed, but the trabecular number remained more or less constant with no significant change. The increase in trabecular volume at an early age is due to increase in the trabecular thickness. This is due to increasing body weight of the growing animal and mechanical loading on the appendicular skeleton (Ruimerman *et al* 2005). However, there is a gradual decline in the connectivity of the trabecular network as represented by a slow decline in the trabecular pattern factor. The reason for this might be due to re-organisation of the trabecular network towards a greater tensile strength and load bearing, where thinner trabeculae are constantly resorbed and thickening of the existing trabeculae (Glatt *et al* 2007). Previous study Glatt *et al* 2005 suggested an age related decrease in trabecular bone volume in C57BL/6J mice. But our data represents an age related increase in bone volume which contrasts the previous works. Firstly the steady increase in both the trabecular and cortical volume in NOD/SCID mice suggests that they are in a phase of active bone growth mediated by bone modelling rather than remodelling. Normal bone remodelling is a locally coupled phenomenon where there is no net gain or loss in the bone component. However, bone modelling is an uncoupled

activity where there is an overall gain in bone components resulting longitudinal or cross sectional increase in the bone size (Bain *et al* 1993). Secondly the difference in the strain and age groups of mice used between these studies might account for the differential pattern observed. Skeletal maturity occurs when there is cessation in the longitudinal and cross-sectional increase in bone size which is at about 16 weeks (Haston *et al* 2008). However, the maximum age group analysed in our present study was 14 weeks and in active bone growth (modelling). Therefore a potential drawback of this study is the failure to assess the age of sexual maturity in the NOD/SCID strain due to the limited time period and age group of mice used.

Age related changes in females followed a similar pattern like their male partners with an increase in the trabecular volume. The change in the trabecular structure and architecture were similar to males at early time points. We observed a more plate-like structure of the trabeculae which are less connected in females compared with males after 7 weeks. This difference might be due to the gonadal sex hormones as the mice attain sexual maturity at 7 weeks (Matsumoto *et al* 2006). The age related changes in the gonadal sex hormone concentration in mice is not well established. Matsumoto *et al* 2006 demonstrated the role of androgen in the osteoblast regulation and bone formation in sexually mature male mice. The rapid decline in SMI in females may be due to active remodeling resorbing thinner trabeculae and the existing trabeculae become thicker and more plate-like. However in males, we suggest that the steady state of the SMI and a gradual decline in the Tb.pf may be the result of comparatively slow remodeling activity due the protective effect of androgens. An obvious increase in the cortical volume of the tibial metaphysis was observed among the females while no such effects were seen among the males. Glatt *et al* 2005 suggested a differential pattern in the modelling and remodelling between different skeletal sites. Moreover the small time frame of 5 to 14 weeks would not be sufficient enough to reflect every significant change in the bone structure and architecture.

In vertebrae, the age related increase in the trabecular volume and trabecular thickness was similar to the appendicular skeleton. There was a significant increase in the trabecular number in both male and female vertebrae, unlike in the tibia where no significant increase in the trabecular number was observed. Although the trabecular volume and thickness were similar to the appendicular skeleton, a

more rapid decline in the Tb.pf and SMI was observed in the vertebrae. The difference in the load transfer characteristics might account for the altered trabecular architecture between these two skeletal sites. The trabecular bone in the vertebrae seems to have more plate-like structures when compared to the tibial metaphysis of the same age group. The appendicular skeleton suffers the stress of mechanical loading due to weight bearing and quadripedal locomotion but the mechanical forces acts on the cortical bone more than the metaphysial trabeculae (Glatt *et al* 2005). However in the case of vertebrae, the trabecular bone participates in load bearing and hence the difference in trabecular architecture ((Tommasini *et al* 2005 and Glatt *et al* 2005).

Quantitative determination of bone formation and bone resorption was done using commercially available ELISA kits for PINP and CTX respectively. Both the bone markers showed an inverse co-relation with age. Our data shows that PINP peaked at an early age (5 weeks) followed by a rapid decline at 7 weeks and a steadier pace thereafter. No significant change was observed in the concentration of P1NP after 7 weeks till the end of the study group. Peak concentration of CTX was observed in both the sexes in early time point followed by a rapid decline thereafter. Our results are in accordance with the previous animal and human studies. DeLaurier *et al* 2002, demonstrated the decline in the bone formation and resorption marker in feline cats with the attainment of skeletal maturity A rapid increase in turnover marker during infancy when there is active bone growth followed by reduction in turnover marker when the animal reaches skeletal maturity. Tsutsumi *et al* 2004, described the decline in the bone markers from infancy to puberty observed in female Gottingen minipigs was similar to the pattern of bone turnover markers in humans. Coeverden *et al* 2002, described the early peak in bone turnover markers in the prepubertal time was due to the phase of active bone growth and the rapid decline at the late pubertal stage was the influence on the sex hormones on bone remodeling.

Age related changes in the cellular composition of the tibial metaphysis were determined in 5, 7 and 12 weeks male mice by histomorphometric analysis. Significant reduction in the osteoblast parameters (Osteoblast number and percentage surface occupancy of the osteoblast over the bone) was observed with increase in the age in both endocortical and trabecular surface. Interestingly, a mild increase in the osteoblast surface occupancy was observed at the trabecular surface at 7 weeks inspite of a

lesser osteoblast number when compared with the 5 weeks group. The age related decrease in the osteoblast number and percentage occupancy over the bone surface is associated with the reduction in the growth rate of the trabecular and cortical bone, as reflected in the μCT assessment of the bone volume. Furthermore, the decrease in the bone formation marker PINP concentration with age substantiates the fact that the decrease in osteoblast number was the resultant activity of suppression in bone formation and not the inherent quality of the mouse tibial osteoblasts. A similar phenomenon of decrease in osteoblast proliferation with age was observed in postnatal human calvaria by de Pollack *et al* 1997. A pattern of reduction in osteoclast parameters was observed. However, no significant change was observed in the osteoclast parameters within the study group due to the large SD and the limited time frame of the study group. As the bone in the observed age group were in a phase of modelling i.e., lack of coupling and primarily bone formation, osteoblastic activity is well pronounced. However a little resorption activity might be observed results in a modelling drift and henceforth, bone growth (Bain *et al* 1993). Significant difference in the distribution of osteoclast was observed between the endocortical and trabecular bone surfaces s at 7 weeks. This substantiates that resorption activity is well pronounced in the trabecular region more the cortex of long bones. This is due mechanical loading characteristics in long bones where thinner trabeculae in the secondary spongiosa far from the joint surfaces are more actively resorbed (Glatt *et al* 2005). Moreover this observation is in accordance with the loss of trabecular connectivity with increasing age, as observed by μCT.

The second objective was aimed at studying the early colonizing events of PC3-GFP-Tib3 cells in 5 weeks NOD/SCID mice to the bone following intracardiac injection. Our experiment suggest that initially following tumour cell inoculation a relatively high number of GFP positive green cells were observed both in groups and as single cells in the first 48hrs. A week later significant reduction in the number of cells was observed as only a few survived and the rest were eliminated. Even though we succeeded in demonstrating the successful visualization of the GFP positive cell in the tibia of NOD/SCID mice we were unable to prove that the visualised GFP positive cells were truly PC3 cells and not bone and blood cells emitting auto-florescence (Baschong *et al* 2001). Furthermore, the visualisation in the trabecular region does not necessarily mean that the GFP positive cells are actually in the bone microenvironment. The cells could have been present in the blood vessels of the tibia by sheer chance.

The above two issues can be addressed in future studies by double labelling of the tumour cell and by labelling the blood vessel which will help in the assessment of the spatial orientation of the tumour cell in relation to the blood vessels.

For successful homing and colonization of tumour cells a more conducive microenvironment is a pre-requisite. Previous studies have demonstrated a high tumour take rate in young mice where the rate of bone turnover is higher than older mice. From the above study we observed that the bone turnover rates are high in the early ages (5 weeks) of life in NOD/SCID mice with more osteoblast and osteoclast cells in both the trabecular and endocortical region. There is a steady decrease in the rates of bone growth and bone turnover with increase in the age of the mice. Hence we conclude that, NOD/SCID male mice of 5 weeks age will be an ideal animal model for studying bone metastasis in prostate cancer using xenograft. Following intracardiac injection of PC3-GFP-Tib3 cells, we demonstrated that these cells home to the bone marrow and can been seen up to a week post injection. However, the successful colonization and metastases development depends on a favourable microenvironment, which is unknown at present. Further studies assessing longer time points will be required for answer these questions. But the bone environment of 5 weeks old NOD/SCID mice seems to be a more promising due to high bone turnover rates and more osteoblast and osteoclast cells which are required for tumour spread and metastases development.

## REFERENCE


1. Abkowitz JL, Robinson AE, Kale S, Long MW (2003). Mobilization of hematopoietic stem cells during homeostasis and after cytokine exposure. *Blood* 102, 1249-
2. Angelucci A, Gravina GL, Rucci N *et al.* (2006) Suppression of EGF-R signaling reduces the incidence of prostate cancer metastasis in nude mice. *Endocr Relat Cancer*; 13,197-210.
3. Bain SD, Watkins BA. (1993) Local Modulation of Skeletal Growth and Bone Modeling in Poultry. *J. Nutr.* 123, 317-322.
4. Baschong W, Suetterlin R, Laeng RH (2001) Control of Autofluorescence of Archival Formaldehyde-fixed, Paraffin-embedded Tissue in Confocal Laser Scanning Microscopy (CLSM). *J. Histochem. Cytochem*. 49, 1565-1572.
5. Bastide.C. Bagnis C, Mannoni.P *et al.* (2002) A Nod Scid mouse model to study human prostate cancer. *Prostate Cancer and Prostatic Diseases.* 5, 311-315.
6. Bennett CN, Longo KA, Wright WS, et al. (2005) Regulation of osteoblastogenesis and bone mass by Wnt10b. *Proceedings of the National Academy of Sciences of the United States of America* 102, 3324-3329.
7. Bluoin S, Bsale MS, Chappard D (2005), Rat models of bone metastases. *Clin Exp Metastasis* 22, 605-614.
8. Bogdanos J, Karamanolakis D, Tenta R *et al.* (2003) Endocrine/paracrine/autocrine survival factor activity of bone microenvironment participates in the development of androgen ablation and chemotherapy refractoriness of prostate cancer metastasis in skeleton. *Endocr Relat Cancer*; 10, 279-289.
9. Bonfil RD, Chinni S, Fridman R *et al* (2007a). Proteases, growth factors, chemokines, and the microenvironment in prostate cancer bone metastasis. *Urologic Oncology: Seminars and Original Investigations*; 25, 407-411.
10. Bonfil RD, Dong Z, Trindade Filho JC *et al.* (2007b) Prostate cancer-associated membrane type 1-matrix metalloproteinase: A pivotal role in bone response and intraosseous tumor growth. *Am J Pathol.* 170, 2100 –2111.
11. Carlin BI, Andriole GL. (2000). The natural history, skeletal complications, and management of bone metastases in patients with prostate carcinoma. *Cancer* 88, 2989-2994.
12. Chackal-Roy M, Neiyemer C, Moore M, and Zetter B R (1989) Stimulation of Human Prostatic Carcinoma Cell Growth by Factors Present in Human Bone Marrow. *J. Clin. Invest.* 84, 43-50.
13. Chaoyong MA (2004). Animal Models of Disease. *Modern Drug Discovery* 7, 30-36.
14. Chu K, Cheng C-J, Ye X *et al.* (2008) Cadherin-11 Promotes the Metastasis of Prostate Cancer Cells to Bone. *Molecular Cancer Research*, 6, 1259-1267.
15. Coeverden SCCMv, Netelenbos JC, de Ridder CM *et al.* (2002). Bone metabolism markers and bone mass in healthy pubertal boys and girls. *Clinical Endocrinology*, 57, 107-116.
16. Cooper CR and Pienta JK (2000). Cell adhesion and chemotaxis in prostate cancer metastasis to bone: a minireview. *Prostate Cancer and Prostatic Diseases* 3, 6-12.
17. Cross NA, Fowles A, Reeves K, *et al* (2008). Imaging the effects of castration on bone turnover and hormone-independent prostate cancer colonization of bone. *The Prostate* 68, 1707-1714.
18. de Pollack C, Arnaud E, Renier D, Marie PJ (1997). Age-related changes in bone formation, osteoblastic cell proliferation, and differentiation during postnatal osteogenesis in human calvaria. *J Cell Biochem* 64, 128–139
19. DeLaurier A, Jackson B, Ingham K, *et al* (2002). Biochemical Markers of Bone Turnover in the Domestic Cat: Relationships with Age and Feline Osteoclastic Resorptive Lesions. *J. Nutr.* 132, 1742S-174.

20. Eaton CL and Coleman RE (2003). Pathophysiology of bone metastases from prostate cancer and the role of bisphosphonates in treatment. Cancer Treatment Reviews 29, 189-198
21. Glatt V, Canalis E, Stadmeyer L *et al.* (2007). Age-Related Changes in Trabecular Architecture Differ in Female and Male C57BL/6J Mice. *JBMR* 22, 1197-1207.
22. Gleave ME, Hsieh JT. Gao C et al (1991) Acceleration of human prostate cancer growth in vivo by factors produced by prostate and bone fibroblasts. *Cancer Research.* 51, 3753–3761.
23. Gronthos S, Zannettino ACW (2007) The role of the chemokine CXCL12 in osteoclastogenesis. *Trends in Endocrinology & Metabolism* 18, 108-113.
24. Hall CL, Dai J, van Golen KL, *et al* (2006) Type I Collagen Receptor ({alpha}2{beta}1) Signaling Promotes the Growth of Human Prostate Cancer Cells within the Bone. *Cancer Res* 66, 8648-8654.
25. Hart IR (1982). 'Seed and soil' revisited: mechanisms of site-specific metastasis. *Cancer and Metastasis Reviews* 1, 5-16.
26. Hartmann CA (2006) Wnt canon orchestrating osteoblastogenesis. *Trends in Cell Biology* 16, 151-158.
27. Haston CK, Li W, Li A, *et al* (2008) Persistent Osteopenia in Adult Cystic Fibrosis Transmembrane Conductance Regulator-deficient Mice. *Am. J. Respir. Crit. Care Med.* 177, 309-315.
28. Hill PA, Murphy G, Dochetry AJ et al (1994) The effects of selective inhibitors of matrix metalloproteinases (MMPs) on bone resorption and the identification of MMPs and TIMP-1 in isolated osteoclasts. J Cell Sci 107, 3055-3064.
29. Hill PA. (1998) Bone Remodelling. *British Journal of Orthodontics* 25, 101-107.
30. Hiraga, T., Williams, P. J., Mundy, G.R., Yoneda, T (2001). The Bisphosphonate Ibandronate Promotes Apoptosis in MDA-MB-231 Human Breast Cancer Cells in Bone Metastases. *Cancer Res* 61, 4418-4424.
31. Huss WJ, Maddison LA, Greenberg NM (2001) Autochthonous mouse models for prostate cancer: past, present and future. *Seminars in Cancer Biology* 11, 245-260.
32. Huss WJ, Maddison LA, Greenberg NM (2001) Autochthonous mouse models for prostate cancer: past, present and future. Seminars in Cancer Biology 11,245-260.
33. Imai K, Kobayashi M, Wang J *et al* (1999) Selective secretion of chemoattractants for haemopoietic progenitor cells by bone marrow endothelial cells: a possible role in homing of haemopoietic progenitor cells to bone marrow. *Br. J. Haematol.*, 106, 905–911.
34. Jacob K, Webber M, Benayahu DK, Kleinman H (1999) Osteonectin Promotes Prostate Cancer Cell Migration and Invasion: A Possible Mechanism for Metastasis to Bone. *Cancer Res* 59,4453-4457.
35. Kazunori H, Atsushi T, Chun-Peng L *et al* (2009) PTEN Knockout Prostate Cancer as a Model for Experimental Immunotherapy. *The Journal of urology* 181, 354-362.
36. Keller ET, Zhang J, Cooper CR *et al* (2001) Prostate carcinoma skeletal metastases: Cross-talk between tumor and bone. *Cancer and Metastasis Reviews* 20, 333-349.
37. Keller ET, Zhang J, Cooper CR *et al* (2001) Prostate carcinoma skeletal metastases: Cross-talk between tumor and bone. *Cancer and Metastasis Reviews* 20, 333-349.
38. Koblinski JE, Kaplan-Singer BR, VanOsdol SJ, et al (2005) Endogenous Osteonectin/SPARC/BM-40 Expression Inhibits MDA-MB-231 Breast Cancer Cell Metastasis. *Cancer Res.* 65, 7370-7377.
39. Kollet O, Dar A, Lapidot D *et al* (2007). The Multiple Roles of Osteoclasts in Host Defense: Bone Remodeling and Hematopoietic Stem Cell Mobilization. *Annual Review of Immunology* 25, 51-69.
40. Krane SM (2005). Identifying genes that regulate bone remodeling as potential therapeutic targets. *J. Exp. Med.* 201, 841-843.

41. Lamb DJ, Zhang L (2005) Challenges in Prostate Cancer Research: Animal Models for Nutritional Studies of Chemoprevention and Disease Progression. *J. Nutr.* 135, 3009S-3015.
42. Lehr JE, Pienta KJ (1998). Preferential adhesion of prostate cancer cells to a human bone marrow endothelial cell line. *J. Natl. Cancer Inst.* 90, 118-123.
43. Loberg R. D., LLD, Jason Harwood *et al* (2006) CCL2 is a Potent Regulator of Prostate Cancer Cell Migration and Proliferation. *Neoplasia*; 8(7):578 - 586.
44. Logothetis CJ and Lin S-H (2005). Osteoblasts in prostate cancer metastasis to bone. *Nature Review on Cancer* 5, 21-28.
45. Lu Y, Wang J, Xu Y *et al* (2008) CXCL16 Functions as a Novel Chemotactic Factor for Prostate Cancer Cells In vitro. *Molecular Cancer Research* 6, 546-554.
46. Matsumoto C, Inada M, Toda K, Miyaura C(2006). Estrogen and androgen play distinct roles in bone turnover in male mice before and after reaching sexual maturity. *Bone* 38, 220-226.
47. Meikle MC, Bord S, Hembry RM, et al (1992) Human osteoblasts in culture synthesize collagenase and other matrix metalloproteinases in response to osteotropic hormones and cytokines. *J Cell Sci* 103, 1093-1099.
48. Mundy GR, Demartino S, Rowe DW (1981) Collagen and Collagen-derived Fragments Are Chemotactic for Tumor Cells. *J Clin Invest.* 68, 1102-1105.
49. Nelson JF, Karelus K, Felicio LS, Johnson TE (1999). Genetic influences on the timing of puberty in mice. *Biology of Reproduction* 42, 649-655.
50. Onganer PU and Djamgoz MBA (2007). Epidermal growth factor potentiates in vitro metastatic behaviour of human prostate cancer PC-3M cells: involvement of voltage-gated sodium channel. *Mol Cancer* 6, 76-88.
51. Paget S (1889). The distribution of secondary growths in cancer of the breast. *Lancet* 1, 571–573
52. Palmieri D, Camardella L, Ulivi V, et al (2000) Carboxyl Propeptide of Collagen I Produced by Mature Osteoblasts Is Chemotactic for Endothelial Cells. *J. Biol. Chem.* 275, 32658-32663.
53. Pfeilschifter J and Mundy GR (1987) TGF-β stimulates osteoblastic activity and is released during the bone resorption process. *Calcium Regulation and Bone Metabolism@ Basic and Clinical Aspects,* 9, 450-454.
54. Pienta KJ, Abate-Shen C,Agus DB *et al* (2008). The current state of Preclinical Prostate cancer Animal Models. *The Prostate 68,* 629-639.
55. Ribatt ID, Mangialardi G, Vacca A (2006). Stephen Paget and the 'seed and soil' theory of metastatic dissemination. *Clinical and Experimental Medicine* 6, 145-149.
56. Ritchie CK, Andrew LR, Thomas KG *et al* (1997) The Effects of Growth Factors Associated with Osteoblasts on Prostate Carcinoma Proliferation and Chemotaxis: Implications for the Development of Metastatic Disease. *Endocrinology* 138, 1145-1150.
57. Roodman GD. Mechanisms of Bone Metastasis. (2004) *N Engl J Med.* 350, 1655-1664.
58. Ruimerman R, Hilbers P, van Rietbergen B, Huiskes R. (2005) A theoretical framework for strain-related trabecular bone maintenance and adaptation. *Journal of Biomechanics.* 38, 931-941.
59. Sasaki A, Boyce BF, Story B, *et al.* (1995) Bisphosphonate Risedronate Reduces Metastatic Human Breast Cancer Burden in Bone in Nude Mice. *Cancer Res.* 55, 3551-3557.
60. Schneider *et al* 2003 In vivo visualization of metastatic prostate cancer and quantitation of disease progression in immunocompromised mice. *Cancer Biol Ther* 2:656–660
61. Shultz LD, Schweitzer PA, Christianson SW *et al* (1995) Multiple defects in innate and adaptive immuno-logic function in NOD/LtSz-scid mice. *J Immunol* 154, 180 – 191.
62. Song Z, Powell WC, Kasahara N, et al (2000) The Effect of Fibroblast Growth Factor 8, Isoform b, on the Biology of Prostate Carcinoma Cells and Their Interaction with Stromal Cells. *Cancer Res.* 60, 6730-6736.

63. Sylvie D, Evelyne G-R, Olivier C, Pierre-Marie M (1996) Divergent effect of TGF&bgr;1 on growth and proteolytic modulation of human prostatic-cancer cell lines. *International Journal of Cancer* 66, 796-801.
64. Taichman RS, Cooper C, Keller ET, Pienta KJ *et al* (2002) Use of the Stromal Cell-derived Factor-1/CXCR4 Pathway in Prostate Cancer Metastasis to Bone. *Cancer Res* 62, 1832-1837.
65. Taichman RS, Loberg RD, Mehra R *et al* (2007). The evolving biology and treatment of prostate cancer. *The Journal of Clinical Investigation* 117, 2351-2361.
66. Takanori S, Toshihiro S, Kohei K, et al (1994) Pattern of prostate cancer metastasis to the vertebral column. *The Prostate* 25, 141-146.
67. Thomas JR, Sarah HT-G, Bruce EL, et al (2003) Animal models of bone metastasis. *Cancer* 97, 748-757.
68. Tommasini Steven M Mtg, Van Der Meulen Marjolein C. H., Jepsen Karl J (2005). Genetic variation in structure-function relationships for the inbred mouse lumbar vertebral body. *JBMR* 20, 817-827.
69. Tsutsumi H, Katagiri K, Morimoto M, *et al* (2004) Diurnal variation and age-related changes of bone turnover markers in female Gottingen minipigs. *Lab Anim* 38, 439-446.
70. Udagawa N(2003) The mechanism of osteoclast differentiation from macrophages: possible roles of T lymphocytes in osteoclastogenesis. *JBMR* 21, 337-343.
71. Vela I, Gregory L, Gardner EM *et al* (2007) Bone and prostate cancer cell interactions in metastatic prostate cancer. *BJU International*. 99, 735-742.
72. Vignery A (2005). Macrophage fusion: the making of osteoclasts and giant cells. *J. Exp. Med.* 202, 337-34.
73. Waters DJ, Sakr WA, Hayden DW *et al* (1998). Workgroup 4: Spontaneous prostate carcinoma in dogs and Non-human primates. *The Prostate* 36, 64-67.
74. Weerden WM and Romijn JC (2000) Use of nude mouse xenograft models in prostate cancer research. *The Prostate* 43, 263-271.
75. Yoneda T. and Hiraga T. (2005). Crosstalk between cancer cells and bone microenvironment in bone metastasis. Biochemical and Biophysical Research Communications 328(3): 679-687.
76. Zaidi M (1990) Calcium receptors on eukaryotic cells with special reference to the osteoclast. *Biosci Rep.*10, 493-507.

# APPENDICES

## APPENDIX I

| Age in week | Male | | | | | | Female | | | | | |
|---|---|---|---|---|---|---|---|---|---|---|---|---|
| | **BV/TV** | **Tb.N** | **Tb.Th** | **Tb.pf** | **SMI** | **BMD** | **BV/TV** | **Tb.N** | **Tb.Th** | **Tb.pf** | **SMI** | **BMD** |
| ***Left tibia*** | | | | | | | | | | | | |
| 5 | 7.58±0.43 | 2.36±0.07 | 0.03±0.001 | 31.31±1.79 | 1.91±0.03 | 1.01±0.01 | 6.37±0.9 | 1.77±0.22 | .035±0.001 | 30.67±3.1 | 1.94±0.13 | 1.05±0.01 |
| 6 | 8.95±0.73 | 2.28±0.16 | 0.03±.0007 | 27.7±6.26 | 1.97±0.16 | 1.04±0.01 | 6.9±3.2 | 1.75±0.67 | 0.03±0.002 | 28.51±9.13 | 1.93±0.33 | 1.08±0.004 |
| 7 | 10.54±1.04 | 2.43±0.38 | 0.04±0.004 | 27.53±7.98 | 2.05±0.25 | 1.07±0.02 | 7.7±0.54 | 1.86±0.17 | 0.04±0.001 | 23.44±1.83 | 1.84±0.08 | 1.11±0.02 |
| 8 | 9.5±1.96 | 2.28±0.43 | 0.04±.0007 | 30.16±4.87 | 2.11±0.17 | 1.1±0.003 | 10.6±2.75 | 2.52±0.65 | 0.04±0.002 | 19.66±4.63 | 1.72±0.19 | 1.10±0.01 |
| 10 | 11.85±3.63 | 2.58±0.75 | 0.04±0.002 | 26.49±4.42 | 2.08±0.19 | 1.13±0.009 | 9.04±1.3 | 1.98±0.30 | 0.04±0.001 | 18.92±1.87 | 1.78±0.05 | 1.13±0.01 |
| 12 | 11.3±1.86 | 2.41±0.43 | 0.04±0.002 | 26.47±1.87 | 2.12±0.10 | 1.17±0.02 | 10.9±1.5 | 2.23±0.30 | 0.05±0.002 | 15.06±3.86 | 1.60±0.2 | 1.14±0.01 |
| 14 | 11.88±2.3 | 2.42±0.46 | 0.04±0.001 | 21.46±5.06 | 1.96±0.24 | 1.13±0.01 | 10.49±3.07 | 2.00±0.54 | 0.05±0.002 | 12.33±4.31 | 1.48±0.27 | 1.14±0.02 |
| ***L1 lumbar Vertebrae*** | | | | | | | | | | | | |
| 5 | 7.73±0.84 | 2.43±1.88 | 0.03±0.003 | 24.65±5.44 | 1.89±0.18 | 0.98±0.03 | 7.87±0.62 | 2.12±2.20 | .035±0.001 | 22.73±5.11 | 1.76±0.21 | 1.03±0.03 |
| 6 | 13.37±0.87 | 3.37±0.29 | 0.03±0.001 | 14.53±2.64 | 1.56±0.09 | 1.07±0.02 | 9.98±3.15 | 2.53±0.67 | .038±0.002 | 17.67±7.31 | 1.64±0.24 | 1.07±0.01 |
| 7 | 11.34±1.82 | 2.95±0.27 | 0.03±0.003 | 14.38±1.82 | 1.66±0.14 | 1.05±0.04 | 10.94±2.03 | 2.81±0.38 | .038±0.003 | 11.84±5.66 | 1.56±0.16 | 1.04±0.04 |
| 8 | 11.84±1.43 | 3.02±0.49 | 0.03±0.002 | 15.12±3.18 | 1.61±0.09 | 1.06±0.03 | 11.00±1.44 | 2.61±0.28 | .041±0.002 | 13.63±3.73 | 1.57±0.16 | 1.07±0.03 |
| 10 | 14.38±1.48 | 2.9±0.29 | 0.04±0.002 | 14.63±1.84 | 1.58±0.12 | 1.07±0.02 | 13.87±2.05 | 3.07±0.57 | .045±0.002 | 8.86±7.19 | 1.41±0.27 | 1.08±0.03 |
| 12 | 13.55±1.04 | 3.08±0.29 | 0.04±0.001 | 12.81±4.07 | 1.47±0.17 | 1.12±0.01 | 12.17±0.87 | 2.77±0.28 | .043±0.001 | 12.91±3.87 | 1.58±0.25 | 1.10±0.01 |
| 14 | 14.22±0.90 | 3.30±0.31 | 0.04±0.002 | 7.45±3.97 | 1.45±0.10 | 1.11±1.09 | 12.14±1.30 | 2.59±0.21 | .046±0.001 | 13.69±1.82 | 1.60±0.08 | 1.13±0.01 |

Trabecular Analysis of Left tibia and L1 lumbar vertebrae of male and female NOD/SCID mice by μCT is given above. Mean ± SD is given for each age group of mice. Each group had 5 animals.

## APPENDIX II

| Bone Marker | Age in weeks | Male | | Female | |
|---|---|---|---|---|---|
| | | Mean | SD | Mean | SD |
| PINP | 5 | 95.3112 | 36.11429 | 30.011 | 10.09045 |
| | 6 | 27.6766 | 7.156537 | 35.4676 | 5.989411 |
| | 7 | 19.0364 | 2.118086 | 13.644 | 2.384861 |
| | 8 | 15.3128 | 5.996828 | 15.0412 | 1.662682 |
| | 10 | 12.2866 | 1.824596 | 11.4524 | 2.717355 |
| | 12 | 7.1224 | 1.868512 | 8.7652 | 1.592122 |
| | 14 | 7.3762 | 1.111967 | 7.5536 | 1.449309 |
| CTX | 5 | 55.0752 | 11.78779 | 48.1574 | 6.276718 |
| | 6 | 32.0342 | 3.332777 | 40.3346 | 10.20959 |
| | 7 | 26.4674 | 3.340608 | 29.5468 | 2.574621 |
| | 8 | 21.3808 | 4.700125 | 33.3098 | 16.16947 |
| | 10 | 25.1168 | 7.574532 | 22.46267 | 3.13439 |
| | 12 | 16.417 | 0.937001 | 22.42633 | 6.344155 |
| | 14 | 17.8266 | 2.297778 | 17.9292 | 2.988249 |

ELISA Analysis for PINP and CTX Bone markers. Results are given as Mean ± SD for each Age group.

# APPENDIX III

## ENDOCORTICAL ANALYSIS

| Age | Location | Ec.Pm (mm) | N.Oc | N.Ob | Oc Pm (mm) | Ob Pm (mm) |
|---|---|---|---|---|---|---|
| 5m1 | A | 1.2876 | 0 | 102 | 0 | 1.2277 |
| | PL | 1.4806 | 0 | 122 | 0 | 1.4219 |
| 5m2 | A | 1.2934 | 3 | 31 | 0.0969 | 0.5065 |
| | PL | 1.3666 | 0 | 110 | 0 | 1.3063 |
| 5m3 | A | 1.5063 | 13 | 16 | 0.4243 | 0.2918 |
| | PL | 1.3979 | 0 | 110 | 0 | 1.3291 |
| 5m4 | A | 1.5379 | 0 | 87 | 0 | 1.156 |
| | PL | 1.3576 | 0 | 137 | 0 | 1.2928 |
| 5m5 | A | 1.4246 | 12 | 42 | 0.3144 | 0.5964 |
| | PL | 1.4667 | 2 | 98 | 0.058 | 1.276 |
| 7m1 | A | 1.2897 | 0 | 52 | 0 | 0.8262 |
| | PL | 1.3314 | 0 | 95 | 0 | 1.1533 |
| 7m2 | A | 1.3781 | 1 | 12 | 0.0549 | 0.1348 |
| | PL | 1.352 | 0 | 90 | 0 | 0.9516 |
| 7m3 | A | 1.3389 | 2 | 26 | 0.0558 | 0.2999 |
| | PL | 1.2711 | 0 | 106 | 0 | 0.9297 |
| 7m4 | A | 1.3099 | 5 | 17 | 0.1068 | 0.2098 |
| | PL | 1.5504 | 2 | 93 | 0.0345 | 1.349 |
| 7m5 | A | 1.5317 | 1 | 13 | 0.0293 | 0.2123 |
| | PL | 1.4689 | 0 | 86 | 0 | 1.0978 |
| 12m1 | A | 1.3798 | 0 | 0 | 0 | 0 |
| | PL | 1.6047 | 0 | 85 | 0 | 1.1818 |
| 12m2 | A | 1.5125 | 1 | 0 | 0.0415 | 0 |
| | PL | 1.6449 | 0 | 42 | 0 | 0.7463 |
| 12m2 | A | 1.539 | 0 | 2 | 0 | 0.0247 |
| | PL | 1.5599 | 0 | 92 | 0 | 1.1954 |
| 12m4 | A | 1.37 | 0 | 0 | 0 | 0 |
| | PL | 1.6421 | 0 | 52 | 0 | 0.7078 |
| 12m5 | A | 1.3091 | 3 | 0 | 0.1204 | 0 |
| | PL | 1.3517 | 2 | 37 | 0.0543 | 0.4576 |

Histomorphometric analysis of Endocortical region for assessment of age related changes in the cellular composition and distribution of bone cells in male NOD/SCID mice.

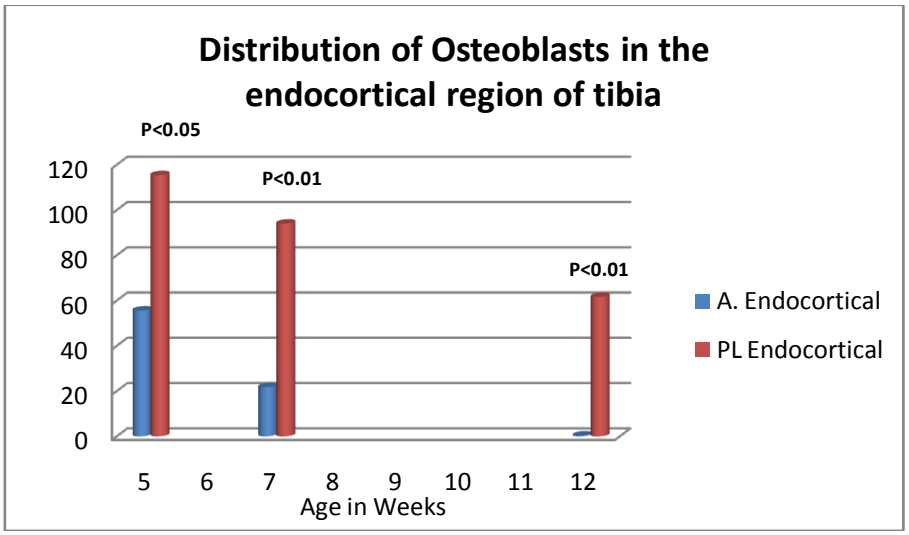


Graph illustrating the difference in the distribution of osteoblast in the anterior and postero-lateral regions of the endocortex in the tibial metaphysis in NOD/SCID mice

The graph shows the distribution of Osteoblast in the anterior and postero-lateral aspect of the endocortical region of the tibial metaphysis of NOD/SCID mice. Significant difference was observed between the distribution of osteoblast with increase in the number of osteoblast up to two folds at 5 weeks rising to 3-4 folds at 7 weeks and 6 folds at 12 weeks of age. A similar phenomenon was observed by Kimmel and Webster 1980, with the non-uniform distribution of osteoblast between two regions at a fixed distance from the growth cartilage metaphysis junction (GCMJ) in the tibial metaphysis of Sprague-Dawley rats where the distribution of osteoblast were much higher in the metaphyseal region closer to the growth cartilage. Several possible explanations were given to this interesting finding. However, the reason for the difference between the anterior and postero-lateral distribution of osteoclast remains unexplained Moreover, the distribution of osteoclast between the anterior and postero lateral endocortical region was not studied as this was not the main objective of interest and could be considered for future analysis. Further studies in different strain of rodents and animal models have to be done to address these questions.

Reference

Kimmel DB, Webster SSJ (1980). A Quantitative Histologic Analysis of the Growing Long Bone Metaphysis. *Calcif. Tissue Int.* 32, 113-122.

# APPENDIX IV

## TRABECULAR ANALYSIS

| Age | N.Ob | N.Oc | Ob Pm (mm) | Oc Pm (mm) | Tb. Pm (mm) |
|---|---|---|---|---|---|
| 5m1 | 49 | 45 | 0.4946 | 5.2826 | 5.2826 |
| 5m2 | 59 | 16 | 0.7155 | 4.3471 | 4.3471 |
| 5m3 | 57 | 8 | 0.8388 | 2.6497 | 2.6497 |
| 5m4 | 223 | 8 | 3.0191 | 7.4278 | 7.4278 |
| 5m5 | 92 | 36 | 1.2615 | 3.687 | 3.687 |
| 7m1 | 208 | 0 | 3.0486 | 6.8471 | 6.8471 |
| 7m2 | 19 | 27 | 0.285 | 3.6707 | 3.6707 |
| 7m3 | 56 | 21 | 1.1237 | 3.1677 | 3.1677 |
| 7m4 | 81 | 23 | 1.6636 | 4.7418 | 4.7418 |
| 7m5 | 38 | 11 | 0.7935 | 2.2576 | 2.2576 |
| 10m1 | 6 | 0 | 0.1018 | 2.2033 | 2.2033 |
| 10m2 | 15 | 6 | 0.2679 | 2.1279 | 2.1279 |
| 10m3 | 16 | 1 | 0.3193 | 1.95 | 1.95 |
| 10m4 | 11 | 0 | 0.135 | 3.0199 | 3.0199 |
| 10m5 | 5 | 18 | 0.0543 | 3.8034 | 3.8034 |

Histomorphometric analysis of the trabecular region in the tibial metaphysis